FZD-485

Experimental investigation and CFD simulation of slug flow in horizontal channels

Christophe Vallée, Thomas Höhne,
Horst-Michael Prasser, Tobias Sühnel

September 2007

Wissenschaftlich-Technische Berichte
FZD-485 2007 · ISSN 1437-322X

WISSENSCHAFTLICH-TECHNISCHE BERICHTE

Forschungszentrum
Dresden Rossendorf

Wissenschaftlich-Technische Berichte
FZD-485
September 2007

Christophe Vallée, Thomas Höhne,
Horst-Michael Prasser, Tobias Sühnel

Experimental investigation and CFD simulation of slug flow in horizontal channels

Technical Report

Forschungszentrum
Dresden Rossendorf

Technischer Fachbericht
Experimentelle Untersuchung und CFD-Simulation von Schwallströmung in horizontalen Kanälen

Technical Report
Experimental investigation and CFD simulation of slug flow in horizontal channels

Reaktorsicherheitsforschung-Vorhaben-Nr./
Reactor Safety Research-project No.: 150 1265

Vorhabenstitel: **Aufbau und Durchführung von Experimenten an der Mehrzweck-Thermohydraulikversuchsanlage TOPFLOW für generische Untersuchungen von Zweiphasenströmungen und die Weiterentwicklung und Validierung von CFD-Codes.**

Project Title: **Construction and execution of experiments at the multi-purpose thermal hydraulic test facility TOPFLOW for generic investigations of two-phase flows and the development and validation of CFD codes.**

Autoren / Author(s): **Christophe Vallée, Thomas Höhne, Horst-Michael Prasser, Tobias Sühnel**

Dienststelle der Autoren / Performing Organisation: **Forschungszentrum Dresden-Rossendorf e.V. Institut für Sicherheitsforschung**

Berichtsdatum / Publication Date: **September 2007**

Berichts-Nr. / Report-No.: **FZD-485**

Das diesem Bericht zugrunde liegende Vorhaben wurde mit Mitteln des Bundesministeriums für Wirtschaft und Technologie unter dem Förderkennzeichen 150 1265 gefördert. Die Verantwortung für den Inhalt dieser Veröffentlichung liegt bei den Autoren.

Berichtsblatt

1. ISBN oder ISSN	2. Berichtsart Technischer Fachbericht
3a. Titel des Berichts Experimentelle Untersuchung und CFD-Simulation von Schwallströmung in horizontalen Kanälen	
3b. Titel der Publikation	
4a. Autoren des Berichts (Name, Vorname(n)) Christophe Vallée, Thomas Höhne, Horst-Michael Prasser, Tobias Sühnel	5. Abschlussdatum des Vorhabens 30.09.2006
	6. Veröffentlichungsdatum September 2007
4b. Autoren der Publikation (Name, Vorname(n))	7. Form der Publikation Broschüre
8. Durchführende Institution(en) (Name, Adresse) Forschungszentrum Dresden-Rossendorf e.V. Institut für Sicherheitsforschung Postfach 510119 01314 Dresden	9. Ber.Nr. Durchführende Institution
	10. Förderkennzeichen *) 150 1265
	11a. Seitenzahl Bericht 48
	11b. Seitenzahl Publikation
13. Fördernde Institution (Name, Adresse) Bundesministeriums für Wirtschaft und Technologie (BMWi) 11019 Berlin	12. Literaturangaben 24
	14. Tabellen 1
	15. Abbildungen 28
16. Zusätzliche Angaben	
17. Vorgelegt bei (Titel, Ort, Datum)	

18. Kurzreferat

Für die Untersuchung von geschichteten Zweiphasenströmungen, wurden am Forschungszentrum Dresden-Rossendorf (FZD) zwei horizontale Kanäle mit rechteckigem Querschnitt gebaut. Diese Kanäle ermöglichen die Untersuchung Luft/Wasser-Strömungen im Gleich- und Gegenstrom bei Atmosphärendruck und Raumtemperatur, insbesondere die Entstehung von Schwallströmungen. Die Teststrecken wurden aus Acrylglas gefertigt, so dass optische Messmethoden angewendet werden können, wie etwa Hochgeschwindigkeits-Videoaufnahmen bzw. die PIV-Technik (particle image velocimetry). Die Auswahl des rechteckigen Querschnitts erlaubt einen optimalen Einsatz dieser Messmethoden. Zudem wurden dynamische Druckmessungen durchgeführt und mit der Hochgeschwindigkeitskamera synchronisiert. CFD Nachrechnungen geschichteter Strömungen wurden mit dem kommerziellen Strömungsberechnungscode ANSYS CFX durchgeführt. Das Euler-Euler Zweifluid-Modell mit der Option für freie Oberflächen wurde auf einem Berechnungsgitter mit $4 \cdot 10^5$ Kontrollvolumen angewendet. Die Turbulenz lies sich mit einem separaten Ansatz für die jeweilige Phase des k-ω basierenden SST Modells (shear stress transport) beschreiben. Die Ergebnisse der Berechnungen stimmen gut im Hinblick auf Schwallentstehung, -geschwindigkeit und Wellenbrechung überein. Diese qualitativ gute Übereinstimmung zwischen Simulation und Experiment ist viel versprechend und zeigt, dass CFD als nützliches Tool zur Beschreibung von horizontalen Zweiphasenströmungen eingesetzt werden kann. Weiterhin wurden Vorrausrechnungen durchgeführt, um den Einsatz des CFD-Codes für Schwallströmungen in einer realen Geometrie und bei Parametern zu zeigen, die für die Reaktorsicherheit relevanten sind. Es wurde ein Zweiphasengemisch von Wasser und Sattdampf bei 50 bar und 263,9°C in einem Modell des Heißstranges eines deutschen Druckwassereaktors (Typ Konvoi) untersucht. Die Ergebnisse dieser Simulation zeigen die Entstehung von Wellen im horizontalen Teil des Heißstranges und deren Anwachsen zu Schwallen im Bogen zum Dampferzeuger.

19. Schlagwörter Horizontale Zweiphasen-Strömung, Phasengrenze, Schwallströmung	
20. Verlag	21. Preis

Document Control Sheet

1. ISBN or ISSN	2. Type of Report Technical Report
3a. Report Title Experimental investigation and CFD simulation of slug flow in horizontal channels	
3b. Title of Publication	
4a. Author(s) of the Report (Family Name, First Name(s)) Christophe Vallée, Thomas Höhne, Horst-Michael Prasser, Tobias Sühnel	5. End of Project 30.09.2006
	6. Publication Date September 2007
4b. Author(s) of the Publication (Family Name, First Name(s))	7. Form of Publication Booklet
8. Performing Organisation(s) (Name, Address) Forschungszentrum Dresden-Rossendorf e.V. Institut für Sicherheitsforschung Postfach 510119 01314 Dresden	9. Originator's Report No.
	10. Reference No.*) 150 1265
	11a. No. of Pages Report 48
	11b. No. of Pages Publication
13. Sponsoring Agency (Name, Address) Bundesministeriums für Wirtschaft und Technologie (BMWi) 11019 Berlin	12. No. of References 24
	14. No. of Tables 1
	15. No. of Figures 28
16. Supplementary Notes	
17. Presented at (Title, Place, Date)	

18. Abstract

For the investigation of stratified two-phase flow, two horizontal channels with rectangular cross-section were built at Forschungszentrum Dresden-Rossendorf (FZD). The channels allow the investigation of air/water co-current flows, especially the slug behaviour, at atmospheric pressure and room temperature. The test-sections are made of acrylic glass, so that optical techniques, like high-speed video observation or particle image velocimetry (PIV), can be applied for measurements. The rectangular cross-section was chosen to provide better observation possibilities. Moreover, dynamic pressure measurements were performed and synchronised with the high-speed camera system. CFD post-test simulations of stratified flows were performed using the code ANSYS CFX. The Euler-Euler two fluid model with the free surface option was applied on grids of minimum $4 \cdot 10^5$ control volumes. The turbulence was modelled separately for each phase using the k-ω based shear stress transport (SST) turbulence model. The results compare well in terms of slug formation, velocity, and breaking. The qualitative agreement between calculation and experiment is encouraging and shows that CFD can be a useful tool in studying horizontal two-phase flow.
Furthermore, CFD pre-test calculations were done to show the possibility of slug flow generation in a real geometry and at relevant parameters for nuclear reactor safety. The simulation was performed on a flat model representing the hot-leg of the German Konvoi-reactor, with water and saturated steam at 50 bar and 263.9°C. The results of the CFD-calculation show wave generation in the horizontal part of the hot-leg which grow to slugs in the region of the bend.

19. Keywords
horizontal two-phase flow, interfacial area, slug flow

20. Publisher	21. Price

This report is part of a series, which comprise following reports:

- Construction and execution of experiments at the multi-purpose thermal hydraulic test facility TOPFLOW for generic investigations of two-phase flows and the development and validation of CFD codes (Final project report), FZD-481,
- Experiments on upwards gas-liquid flow in vertical pipes, FZD-482,
- Experiments on two-phase flow in a vertical tube with a moveable obstacle, FZD-483,
- Experimental investigation of stratified air/water flows in a horizontal channel, FZD-484,
- Experimental investigation and CFD simulation of slug flow in horizontal channels, FZD-485,
- CFD models for polydispersed bubbly flows, FZD-486,
- Turbulent Dispersion of Bubbles in Poly-dispersed Gas-Liquid Flows in a Vertical Pipe, FZD-487,
- Validation of the Multiple Velocity Multiple Size Group (CFX10.0 N x M MUSIG) Model for Poly-dispersed Multiphase Flows, FZD-487.

All these reports are published as reports of the Forschungszentrum Dresden-Rossendorf.

Dieser Bericht ist Teil einer Serie, die folgende Einzelberichte umfasst:

- Aufbau und Durchführung von Experimenten an der Mehrzweck-Thermohydraulikversuchsanlage TOPFLOW für generische Untersuchungen von Zweiphasenströmungen und die Weiterentwicklung und Validierung von CFD-Codes (Abschlussbericht), FZD-480,
- Experimente zu aufwärtsgerichteten Gas-Flüssig Strömungen in vertikalen Rohren, FZD-482,
- Experimente zur Zweiphasenströmung in einem vertikalen Rohr mit verschiebbarem Hindernis, FZD-483,
- Experimentelle Untersuchung von geschichteten Luft/Wasser Strömungen in einem horizontalen Kanal, FZD-484,
- Experimentelle Untersuchung und CFD-Simulation von Schwallströmung in horizontalen Kanälen, FZD-485,
- CFD Modelle für polydisperse Blasenströmungen, FZD-486,
- Turbulente Blasendispersion in einer polydispersen Rohrströmung, FZD-487,
- Validierung des N x M MUSIG Modells für polydisperse Mehrphasen-strömungen, FZD-487.

Alle Berichte sind als Berichte des Forschungszentrums Dresden-Rossendorf veröffentlicht.

Contents

1. Introduction

Slug flow as a multiphase flow regime can occur in the main cooling lines of pressurized water reactors, for instance after a small break Loss of Coolant Accident (LOCA), and also in other fields, like chemical plants or oil pipelines. The slug flow regime is usually characterized by an acceleration of the gaseous phase and by the transition of fast liquid slugs, which carry a significant amount of liquid with high kinetic energy. It is potentially hazardous to the structure of the system due to the strong oscillating pressure levels formed behind the liquid slugs as well as the mechanical momentum of the slugs.

For the experimental investigation of air/water flows, two horizontal channels with rectangular cross-section were built at *Forschungszentrum Dresden-Rossendorf* (FZD). The first channel, allowing co- and counter-current flows, was used for preliminary studies. As some uncertainties were noticed at the inlet of the test-section, the HAWAC (Horizontal Air/Water Channel) dedicated to co-current flows was built. Its improved inlet device provides defined inlet boundary conditions. Both channels allow in particular the study of air/water slug flow under atmospheric pressure.

Parallel to the experiments, CFD calculations were carried out. The aim of the numerical simulations is the validation of prediction of the slug flow with the existing multiphase flow models built in the commercial code *ANSYS CFX*. Further it is of interest to prove the understanding of the general fluid dynamic mechanism leading to slug flow and to identify the critical parameters affecting the main slug flow parameters (like e.g. slug length, frequency and propagation velocity; pressure drop).

2. Previous modelling of slug flow

According to Manfield (2000), only few attempts using CFD to study slug flow have been made. He simulated a single, isolated liquid slug using a three-dimensional CFD Volume-of-Fluid (VOF) method. Three models of varying complexity were developed: a simulation of the tail of an “infinitely long” slug, a model of short slug whose front is represented by a solid barrier and a simulation of a slug front as a gas-liquid interface.

Other groups have also reported studies of slug flow using CFD. Mao and Dukler (1991) wrote a dedicated CFD programme to simulate the liquid flow around a Taylor bubble in vertical flow. Pan (1996) reported that this was limited in ability and flexibility. Issa and Tang (1990) used a similar approach, also for vertical flow. Moe (1992) simulated the propagation of elongated bubbles in channels initially filled with liquid, closed at one end and open to the atmosphere at the other. Moe also simulated the motion of a single bubble in a pipe containing stagnant liquid, but did not extend this to systems with a net liquid flow. Ubbink (1997) included a case study of the shape and rise velocity of Taylor bubbles in vertical flow as part of his general investigation into the modelling of gas-liquid interfaces. He used a moving-wall boundary condition and simulated a “wedge” of axisymmetric vertical flow. The initial position of the interface was taken from experimental observations and Ubbink simulated the development of the interface shape with time.

Recently, Anglart and Podowski (2002) investigated the fluid mechanics of Taylor bubbles and slug flows in vertical, circular channels using detailed, three-dimensional CFD simulations. The Volume-of-Fluid model with the interface-sharpening algorithm, implemented in the commercial *CFX-4* code, was used to predict shape and velocity of Taylor bubbles moving along a vertical channel. Several cases were investigated, including both a single Taylor bubble and a train of bubbles rising in water. The computer simulations that were performed revealed the importance of properly modelling the three-dimensional nature of phenomena governing the motion of Taylor bubbles.

Lun et al. (1996) used the commercial CFD programme FIDAP to simulate the growth of a wave on the interface of two immiscible fluids with different properties in horizontal stratified gas-liquid flow. The method used to simulate the liquid surface was not described. A coarse two-dimensional grid was developed to represent the flow domain. Significant numerical instabilities during the calculation led to convergence difficulties. These were ascribed to the coarseness of the meshes. Results show the growth of a wave until it completely broaches the pipe and thus initiates slug flow. However, it seems unlikely that the simulated wave growth was completely unbiased by the numerical instabilities.

A three-dimensional slug flow study has been performed by Ujang (2003) for the movement of large Taylor bubbles in a downward inclined pipe. The free surface simulation was conducted using a moving wall boundary. By adjusting the wall speed in accordance with the Taylor bubble rise velocity, the bubble front could be artificially frozen in the computational domain and detailed studies on the formation of the bubble front could be carried out. Close agreement was obtained with air-water

experimental data in a 1-inch diameter pipe for a downward angle of -15° and for different fluid velocities.

A systematic study of numerical simulation of slug flow in horizontal pipes using CFX-5 was carried out by Frank (2003). It was shown that the formation of the slug flow regime strongly depends on the wall friction of the liquid phase. In simulations using inlet/outlet boundary conditions it was found, that the formation of slug flow regimes strongly depends on the agitation or perturbation of the inlet boundary conditions. Furthermore Frank showed that the length of the computational domain plays an important role in slug formation.

Experimental data was delivered by Woods and Hanratty (1999) for a horizontal pipeline with a diameter of 76.3 mm and a length of 20 m. The Perspex pipe segments make it possible to film the flow. Further, liquid holdup and dynamic pressure were measured. Similar experiments were performed by Soleimani and Hanratty (2003) for a 18.3 m long pipe of 25.4 mm diameter.

Nevertheless, the direct comparison between CFD calculations and measurements of the slug generation mechanisms and its propagation in horizontal pipes was not analysed. The recent improvements of the multiphase flow modelling in the *ANSYS CFX* code make it now possible to simulate in detail these mechanisms. In order to validate the implemented models, high-resolution measurement data is needed in time and also in space. Thanks to the optical access of the test channels built at Forschungszentrum Rossendorf, it is possible to study detailed local stratified air/water flow phenomena. These experimental results give an important input for two-phase flow CFD model validation (i.e. interfacial momentum transfer, turbulent profiles of each phase).

3. CFD model with time-dependent inlet boundary conditions for slug generation in a short channel

3.1 The horizontal channel with a separator at the inlet

Experiments were carried out at a horizontal duct mounted between two separators (Fig. 3.1). This configuration allows both co-current and counter-current flow experiments. The two-meter long acrylic glass test section has a rectangular cross-section (height x width: 250 x 50 mm²).

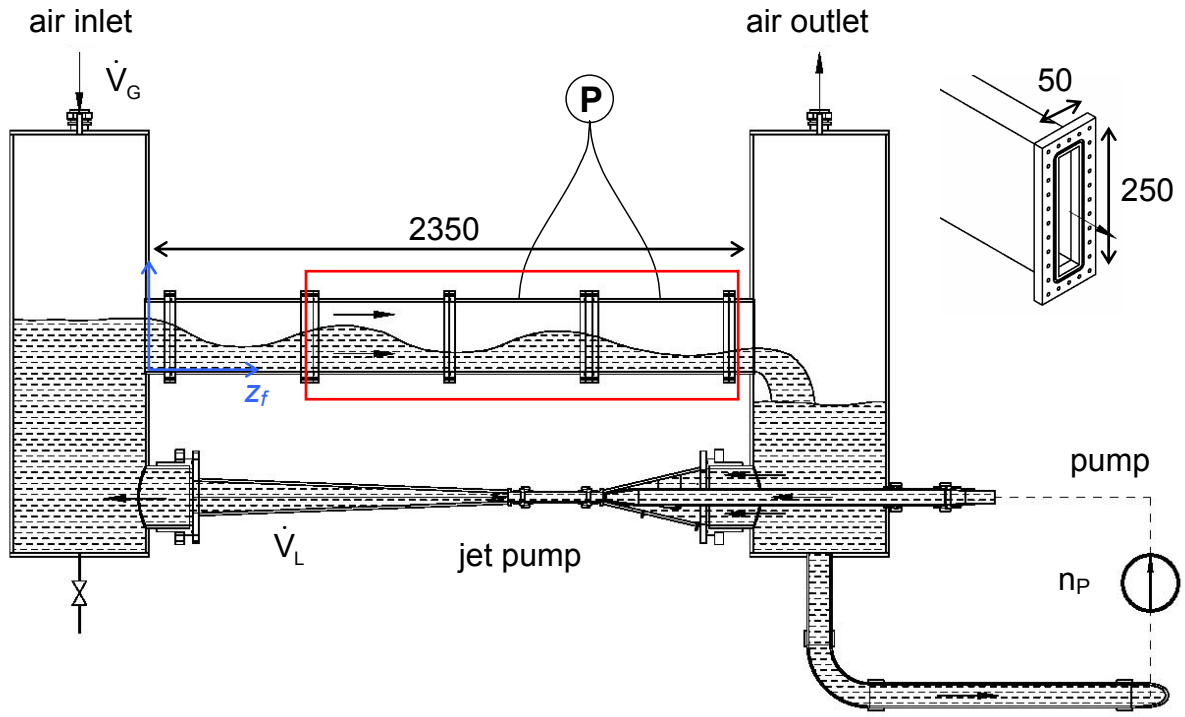

Fig. 3.1: Schematic view of the horizontal channel with inlet separator and modelled part (red)

The flow rates for both air and water are controlled separately by:

- an air flow controller in a range of up to 1650 l/min (i.e. 2.2 m/s superficial velocity in the test section);
- a frequency transformer for the pump motor to control the water flow rate.

A jet pump is driving the water flow, while the air is being injected at the top of one of the separators depending on the type of experiment (co-current or counter-current flow). The directly pumped water flow rate is measured by an ultrasonic flow meter, which is based on the sound wave propagation time measurement. A jet pump is used to amplify the water flow rate in order to enhance the operation range of the facility. The increase of the water flow rate in the jet pump is calculated from the dynamic pressure difference measured at two positions within the convergent part of the jet pump. The best-achieved amplification factor of the jet pump (i.e. the total water flow divided by the directly pumped water flow) was about 1.8. The maximum total water flow rate reaches about 10 l/s (i.e. 0.8 m/s superficial velocity), whereas the measurement accuracy is about ±10%.

First tests have shown that in co-current mode the flow rates are sufficient to establish the following flow regimes: stratified flow (smooth and wavy flows), slug flow and elongated bubble flow.

Due to the rectangular cross-section, the flow can be observed very well from the side of the duct. So, optical techniques, like high-speed video observation and particle image velocimetry (PIV) can be applied to record the flow pattern and to extract quantitative information. For dynamic pressure measurements, piezoelectric transducers were mounted on top of the duct. Their data acquisition system was synchronised with the high-speed video camera.

3.2 Interface capture

3.2.1 Interface capture method

To make quantitative observations, the flow was filmed with a high-speed video camera from the side of the duct (see Fig. 3.2, corresponding to the modelled region of Fig. 3.1). Then the pictures have been analysed to capture the gas-liquid interface.

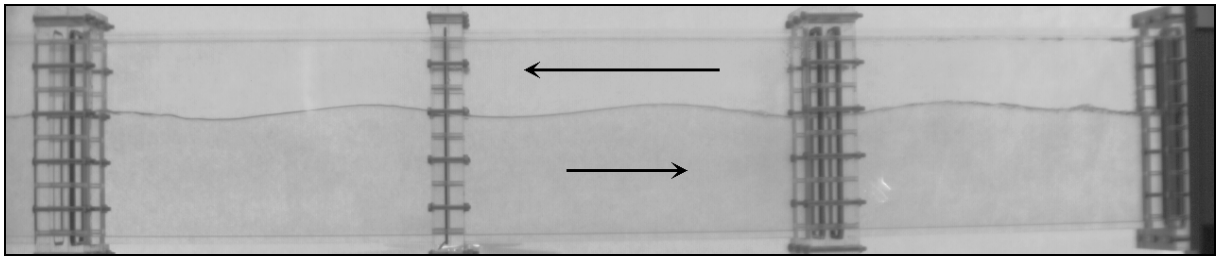

Fig. 3.2: Example of an image taken from the high-speed camera during counter-current stratified wavy flow (superficial velocities: J_L = 0.14 m/s; J_G = -2.2 m/s)

The capture method consists in the following steps:

1. a background subtraction with an image of the completely filled duct;
2. a pixel detection in each vertical line:
   - of the darkest pixel;
   - of the minimum of a grey-level time variation;
3. picking out of the pixels detected in step 2, the one which fits best into a continuous interface line (see Fig. 3).

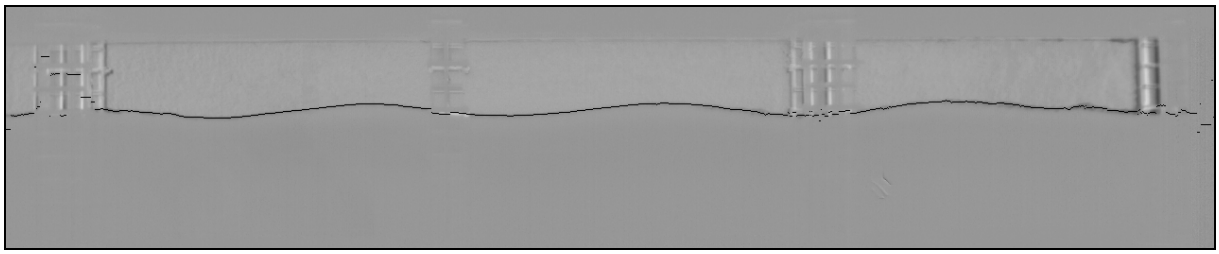

Fig. 3.3: Detected interface line for the image given in Fig. 3.2 with subtracted background

Finally, the interface is represented by a water level as function of the duct length *z* and the time *t*: *h(z, t)*. The spatial resolution of the pictures is about 1.1 mm/pixel.

The accuracy of the interface detection algorithm depends on the thickness of the interface in the images, which is less than 6 pixels for most of the observed stratified flows. Therefore, the accuracy of the water level measurement is about ±3 pixels (i.e. ±3.4 mm).

3.2.2 Water level history during slug flow

The superficial velocities of the modelled slug flow (see Fig. 3.4) were as follows: 0.69 m/s for the water flow (i.e. 8.68 l/s) and 2.2 m/s for the air flow (i.e. 1650 l/min).

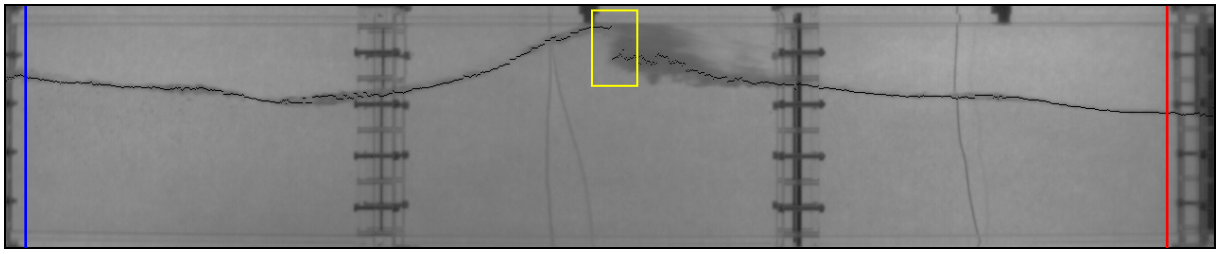

Fig. 3.4: Slug flow - studied cross-sections (blue and red lines) and characteristic interface step (yellow box)

The water level in a cross-section as a function of time can be extracted from the function $h(z, t)$ by keeping z constant. The accuracy of the water level detection is in the range mentioned above except in the region of the slug front, where the definition of a water level is difficult due to the generated two-phase mixture. Fig. 3.5 shows the resulting water level history for the two cross-sections indicated in Fig. 3.4, whose axial positions are as follows:

- at z_f = 0.75 m, after the first flange (left line in Fig. 3.4);
- just before the duct outlet, at z_f = 2.17 m (right line in Fig. 3.4).

The water level was measured with a frequency of 100 Hz, which corresponds to the frame rate of the high-speed camera. From Fig. 3.5 can be seen that the average water level decreases in flow direction because of the pressure drop of approximately 500 Pa. Each slug passing the cross-sections is recognised by a significant peak marked by the boxes. After the passage of the slug, the water level decreases by about 50 mm compared to the level in front of the slug. Then it is increasing slowly until it reaches the critical level and the next slug appears. This phenomenon also shows that a slug expels a significant amount of water from the duct to the second separator.

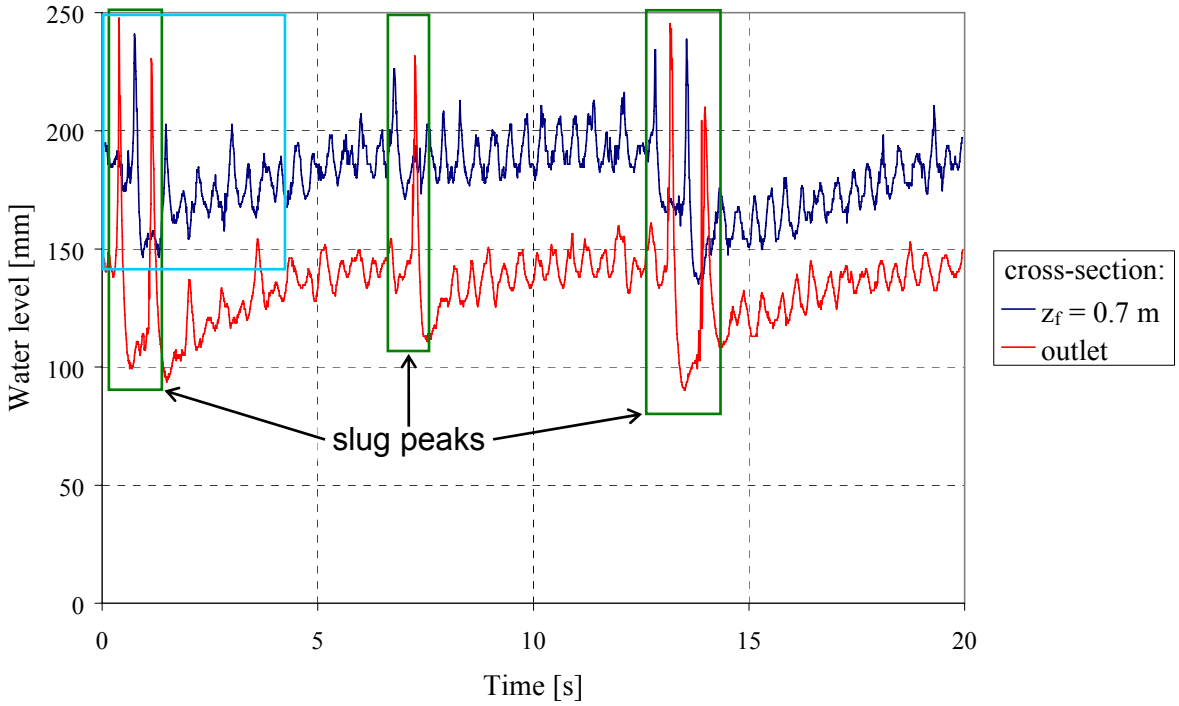

Fig. 3.5: Time-dependent water level during slug flow (measuring frequency: 100 Hz)

3.3 CFD model of the duct

3.3.1 Flow solver

The CFD calculation was performed using the software package *CFX-5.7* (*ANSYS CFX*, 2004). The main characteristics of the solver are:

- Finite element based finite volume method for hybrid unstructured meshes;
- Coupled solver for momentum and mass;
- Implicit pressure based formulation;
- Co-located variables;
- Algebraic multi-grid method;
- High parallelisation;
- A selection of different time and space discretization schemes;
- Availability of different turbulence models (*k-ε* model, *k-ω* model, SST model, Reynolds stress models, LES with Smagorinsky subgrid model);
- Multi-phase formulations: Lagrangian particle tracking, homogenous multi-phase model, Euler-Euler multi-phase formulation (particle model, mixture model).

3.3.2 Multiphase flow model

For slug flow simulations in horizontal pipes and channels, an appropriate multiphase flow model has to be selected in combination with the *ANSYS CFX* free surface model. Due to the geometrical scale of the horizontal channel it is not possible to resolve the spatial structure of the free surface into the micro-scale with the CFD

model. A slug flow simulation can therefore not cover onset and evolution of Kelvin-Helmholtz instabilities at the free surface. The interface drag law applied to the location of the free surface must consider the influence of these free surface instabilities on the macro-scale flow properties. Additionally, the movement of the free surface at the inlet boundary condition introduces instabilities.

For free surface simulations, the inhomogeneous multiphase model recommended by Frank (2003) was used, where the gaseous and liquid phases can be partially mixed in certain areas of the flow domain. In this case, the local phase demixing after gas entrainment is controlled by buoyancy and interphase drag and is not hindered by the phase interface separating the two fluids. A surface capturing method using a compressive advection scheme is used in *ANSYS CFX*. Explicit interface tracking methods (e.g. VOF or Level Sets methods) were not applied. A further decision has to be made regarding the applied fluid morphology and interphase drag law for the multiphase flow. The total drag force F_d is most conveniently expressed in terms of the dimensionless drag coefficient C_D,

$$F_d = \frac{1}{2} \cdot \rho_{LG} \cdot \left(U_L - U_G\right)^2 \cdot A \cdot C_D \tag{3.1}$$

where ρ is the fluid density, (U_L - U_G) is the relative speed and A is the projected area of the interphase in flow direction. In (1), L describes the liquid phase and G the gaseous phase.

The interfacial length scale was set to d_{LG} = 0.001 m, according to a similar assumption made by Frank (2003). The drag law for slug flow was taken from Ishii (1990, p. 37) and the model constant was fixed to C_D = 0.44. The surface tension coefficient was set to 0.072 N/m.

3.3.3 Turbulence modelling

Generally, it is possible to apply a homogeneous turbulence model to both phases. In this study, the fluid-dependent shear stress transport (SST) turbulence models (Menter, 1993) were selected for each phase. Damping of turbulent diffusion at the interface has not been considered. The k-ω based SST model accounts for the transport of the turbulent shear stress and gives highly accurate predictions of the onset and the amount of flow separation under adverse pressure gradients. The SST model combines the advantages of the Wilcox (1994) and of the k-ε model.

To take buoyancy effects into account, a buoyancy production term was used in the turbulence model and was included in the k- and ω-equations for additional turbulence production and dissipation. If the full buoyancy model is being used, the buoyancy production term P_{kb} is modelled according to *ANSYS CFX* (2004) as:

$$P_{kb} = -\frac{\mu_t}{\rho \cdot Pr_t} \cdot \vec{g} \bullet \nabla \rho \tag{3.2}$$

where ρ is the density of the fluid, Pr_t the turbulent Prandtl number, μ_t the turbulent viscosity and $\vec{g}$ the gravity vector.

3.4 Geometry, grid generation and boundary conditions

3.4.1 Geometry and grid generation

Due to very high numerical efforts of transient slug flow simulations, the modelling of the complete test facility is not feasible. In order to keep computational time within acceptable limits, only the horizontal test section with its rectangular cross-section was modelled. The model dimensions are: length x height x width = 2000 x 250 x 50 mm³. The grid was created with *CFX-MESHBUILD* and transferred to *CFX-5 PRE* (Fig. 3.6). It consists of $4x10^5$ hexahedral elements (number of nodes: length x height x width = 400 x 100 x 10), which reduces the computational time and improves the quality of the mesh compared to tetrahedrons. Two different grid densities were studied.

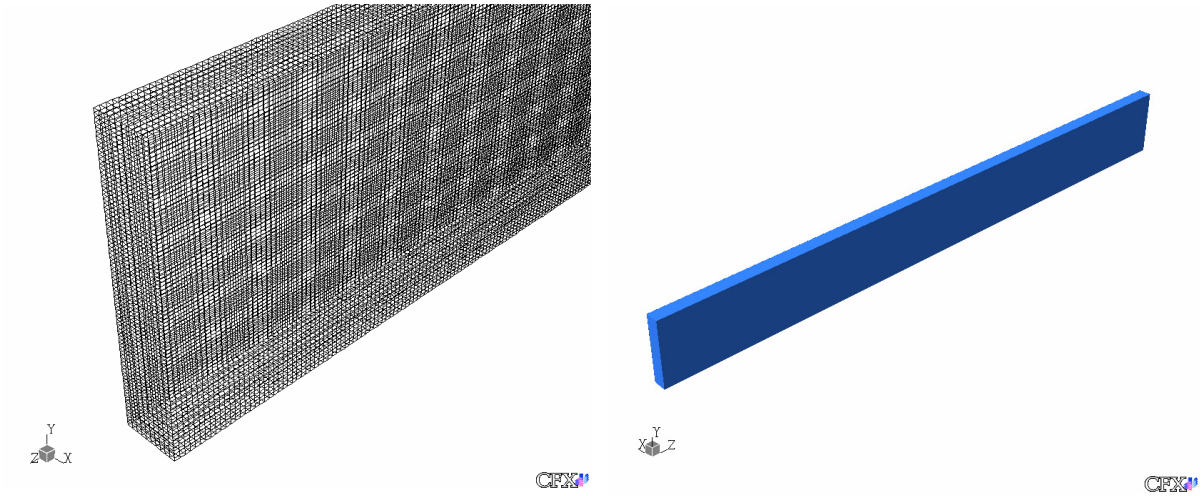

a) Mesh density b) Fluid domain (channel)

Fig. 3.6: CFD model of the duct

3.4.2 Fluid properties, boundary and initial conditions

The gaseous phase is air and the liquid phase is water, both at 25°C and at a reference pressure of 1 bar. The phases have been treated as isothermal and incompressible. Buoyancy effects between the two phases are taken into account by the directed gravity term.

In the experimental setup the inlet boundary conditions into the horizontal channel are not constant. Especially the liquid and gas velocities depend on the conditions before the entrance into the channel. Therefore, the inlet boundary conditions of the CFD calculation (water level, water mass flow rate and air mass flow rate) should be time-dependent. For the calculation, air and water velocities were set to constant values over the whole inlet cross-section (at z_m = 0.0 m). The test conditions of the recalculated slug flow experiment were as follows: water flow of 8.68 l/s and air flow of 1650 l/min. In accordance with these conditions and the initial water level of 194 mm, the inlet velocities were set to 8.93 m/s for the air phase and to 0.895 m/s for the water phase. These velocities were kept constant during the simulation. The turbulent kinetic energy and dissipation rate at the inlet were set to the standard values of *ANSYS CFX*.

Thanks to the interface capture, the water level history of the recalculated experiment is known at z_f = 0.75 m (see paragraph 3.2.2 and Fig. 3.5). At this position, the

influence of the duct inlet geometry on the flow is not so prominent anymore. For this reason, the experimental water level history measured at z_f = 0.75 m (see the blue curve in Fig. 3.5) was used as time-dependent boundary condition for the calculations at the inlet cross-section (at z_m = 0.0 m) of the modelling domain.

A pressure controlled outlet boundary condition has been applied to the cross section at the other end of the horizontal channel (at z_m = 2.0 m). The inner surface of the channel walls has been defined as hydraulically smooth with a non-slip boundary condition applied to both gaseous and liquid phases.

In accordance with the experiment, the initial water level and therefore the entire free surface was set to y_0 = 0.194 m, so the liquid phase covers 78% of the channel (see Fig. 3.7-a). A hydrostatic pressure was assumed for the liquid phase (see Fig. 3.7-b).

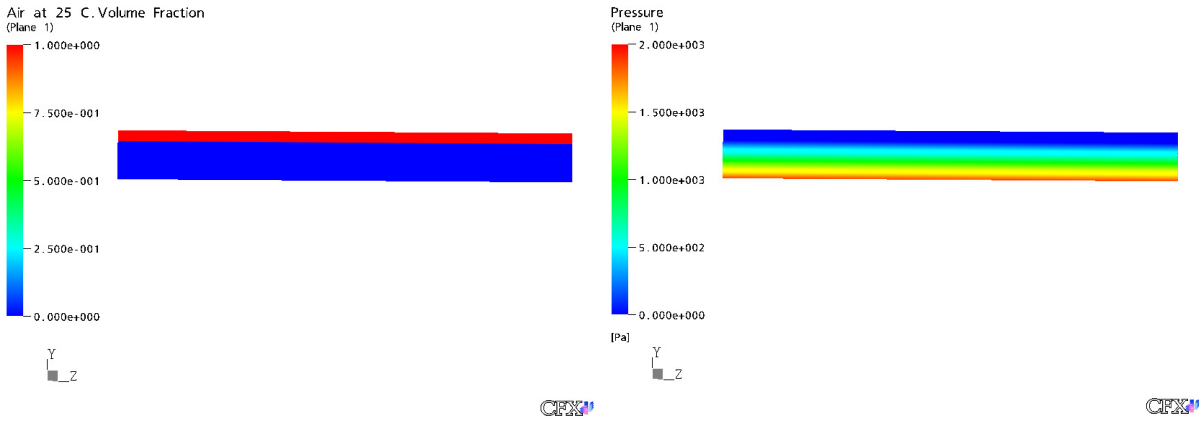

a) Air volume fraction, initial state [-] b) Hydrostatic pressure, initial state [Pa]

Fig. 3.7: Initial conditions of the mass fractions and the hydrostatic pressure in the channel

3.4.3 Discretization schemes, time step and convergence

The parallel transient calculations on 4 processors lasted 3 weeks on a 76 processor *MSC-LINUX* cluster (dual CPU compute nodes at 3.2 GHz, each containing 2 GB RAM).

Due to the high numerical efforts for the transient slug flow simulation, it was not possible to carry out a full numerical study including the evaluation of the dependence of numerical solutions on time integration method, time steps and convergence criteria according to the Best Practice Guidelines (Menter, 2002).

A high resolution discretization scheme was used. For time integration, the fully implicit second order backward Euler method was applied with a constant time step of dt = 0.001 s and a maximum of 15 coefficient loops. A convergence in terms of the RMS values of the residuals to be less than 10^{-4} could be assured most of the time.

3.5 Results

3.5.1 Qualitative results

The picture sequence (see Fig. 3.8) shows the flow observed during the experiment in comparison to the corresponding CFD calculation. Since the filmed test section

length and the modelled part of the channel are different, the last part of the model can not be compared with experimental data. This explains the length difference between the camera frames and the visualisations of calculation results in Fig. 3.8.

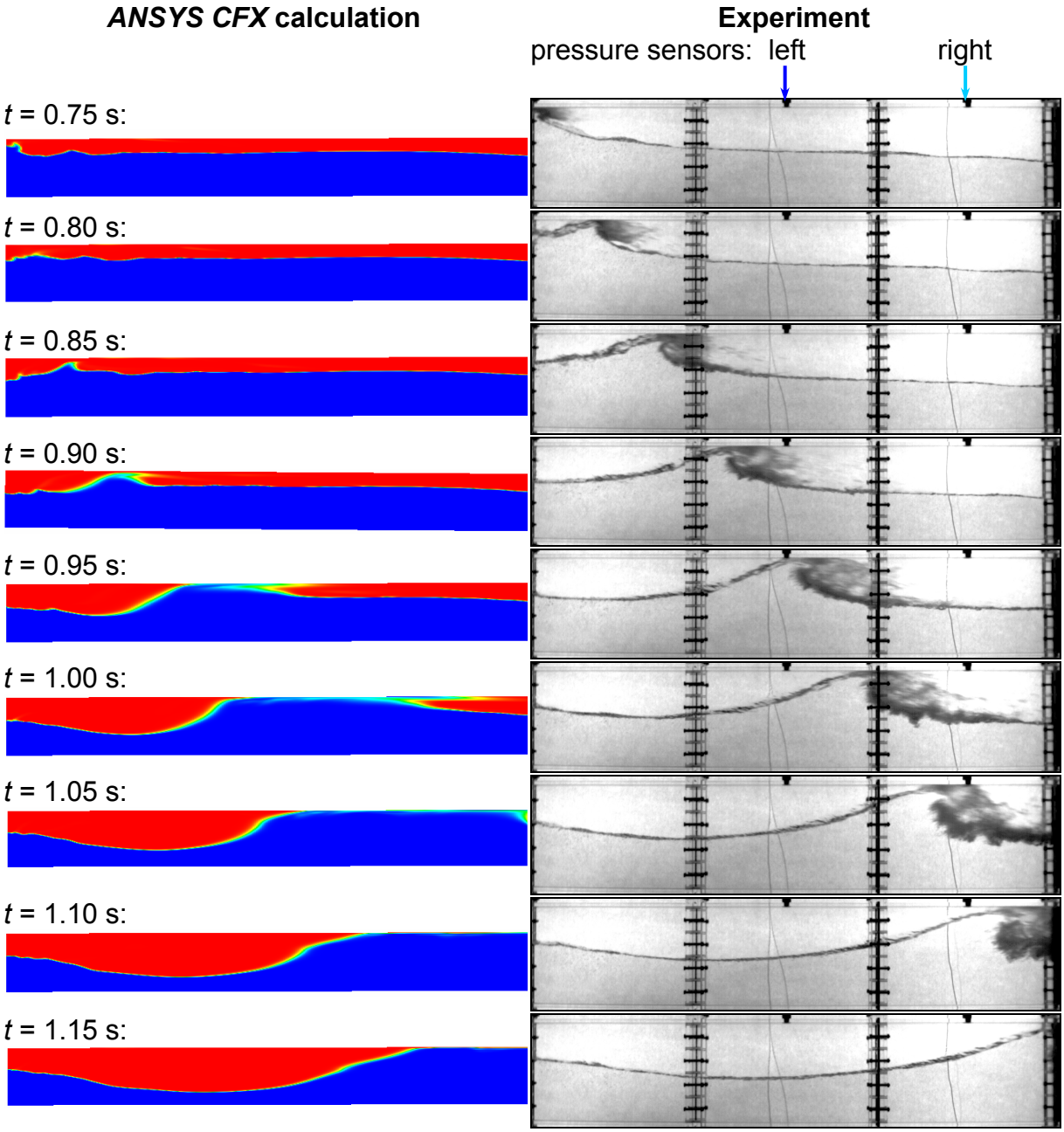

Fig. 3.8: Measured and calculated image sequences at slug flow conditions

In both cases, a slug is developing. In the CFD calculation, the slug develops approximately at t = 0.90 s due to a high peak of the experimental water level at the inlet cross-section of the model. The tail of the calculated slug and the flow behind it is in good agreement with the experiment. The entrainment of droplets in front of the slug could not be observed in the calculation. However, the rolling over and breaking of the wave, characteristic of a slug, are clearly to be seen in Fig. 3.8. These are created by the shear generated by the high air velocity.

In contrast to the measurement, the slug length is increasing in time in the calculation. This could be a result of the different amount of water in the channel at the beginning of the experiment and the simulation. While in the simulation, the liquid phase covered 78% of the channel, it represented about 70% at the beginning of the experiment. Furthermore, in the experiment, this value was also reduced by a first slug, which carried a significant amount of water out of the channel. This first slug could not be simulated. This is probably an effect of the simplified initial conditions assumed in the calculation. Because of the constant initial water level, it took quite a long simulation time to establish a wavy flow along the channel, which is necessary for slug formation. Whereas at the beginning of the measurements, the test channel was already in a fully established intermittent slugging regime.

3.5.2 Slug propagation across the duct

The slug position was extracted from the experimental pictures after an interface capture. Since the interface capture algorithm detects only one pixel in each vertical line, the interface function always presents a discontinuity where the slug is rolling over (c.f. the yellow box in Fig. 3.4). This point was considered as the slug axial position.

As remarked in the previous paragraph, the visualised calculation results show that the slug gains length continuously. For this reason, the slug front propagates significantly faster than its tail, which is in a qualitative good agreement with the experiment. Therefore, the slug position was taken as the first axial position (from the left) where the recalculated slug reaches the top of the duct.

The slug axial position obtained in this way was plotted in function of time in Fig. 3.9 for both experiment and simulation. This was performed with an accuracy of about ±30 mm. As shown in Fig. 3.9, in the experiment the slug moves along the duct with a constant velocity, in average at 3.7 m/s.

The slug propagation of CFD calculation is divided into two characteristic parts:

- between 0.75 and 0.90 s, as the slug is still in preparation, the wave which is generating the slug is accelerating (doted part of the red line in Fig. 3.9).
- from t = 0.90 s, when the wave blocks the whole cross-section of the channel, the slug propagates with a nearly constant velocity in the calculation, too. The average velocity of the calculated slug is 4.4 m/s, which is 18% higher than in the experiment.

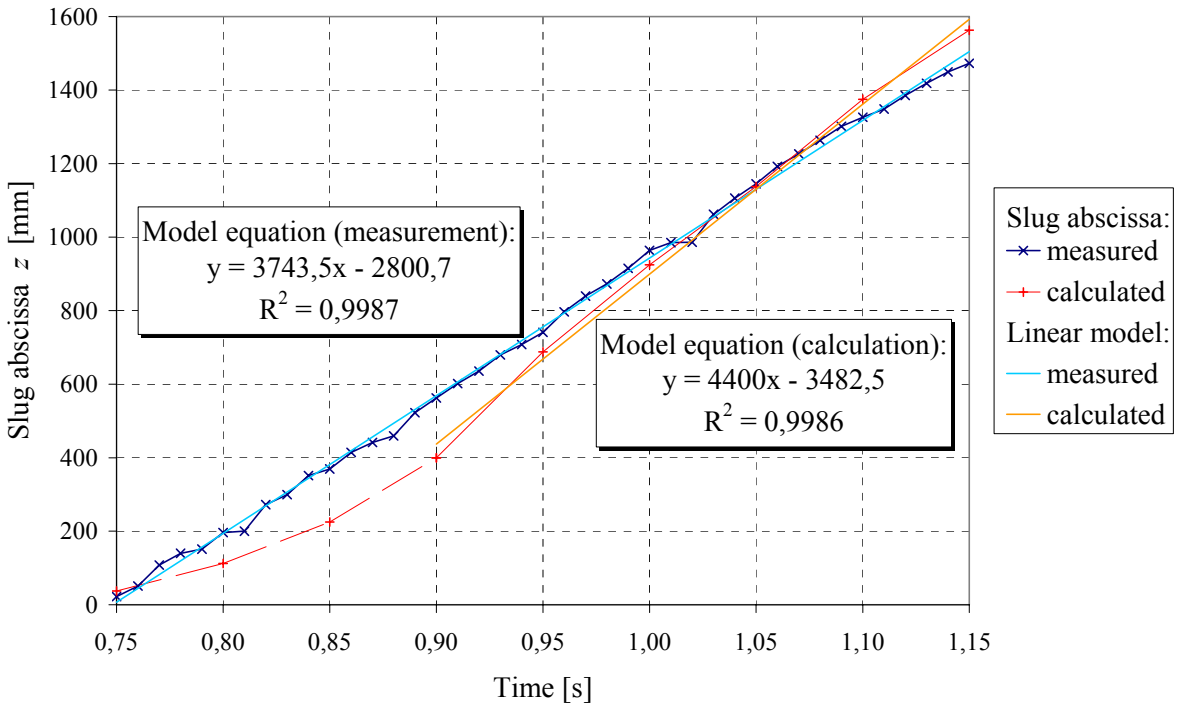

Fig. 3.9: Propagation of a slug - comparison between measurement and calculation

3.5.3 Dynamic pressure

a. Pressure measurements

Since slug flow is a transient phenomenon, suitable pressure sensors have to be fast. That is why existing piezoelectric pressure transducers with a rise time of 2 µs were chosen. They were mounted on top of the last two sections of the duct (i.e. at z_f = 1.45 m and 1.95 m, c.f. Fig. 3.1). Moreover, the pressure measurements were synchronised with the high-speed video camera system. A disadvantage of the piezoelectric transducers is the drift due to the discharge time of the quartz crystals. This causes a static error of about 20%. Unfortunately, alternatives were not available for the present studies.

A typical pressure measurement of a slug flow is shown in Fig. 3.10. The maximum pressure level behind a slug varies from slug to slug, but it is typically in the order of kilopascals.

The zoom in on the first slug passage shows that the pressure increases rapidly: typical rise times are 2 ms (left sensor) and 10 ms (right sensor). An analysis of the camera pictures taken during the pressure measurements could explain the large spectrum of rise times. They are in fact an indicator of the slug length: the longer the slug, the longer the rise time. This means that in the presented measurement (Fig. 3.10), the slug has grown between the two sensors. The pressure decreases simultaneously on both measuring positions. The time of about 20 ms needed to reach atmospheric pressure again, is longer than the rise time. The pictures taken by the camera show that the pressure decreases when the slug leaves the duct towards the outlet separator.

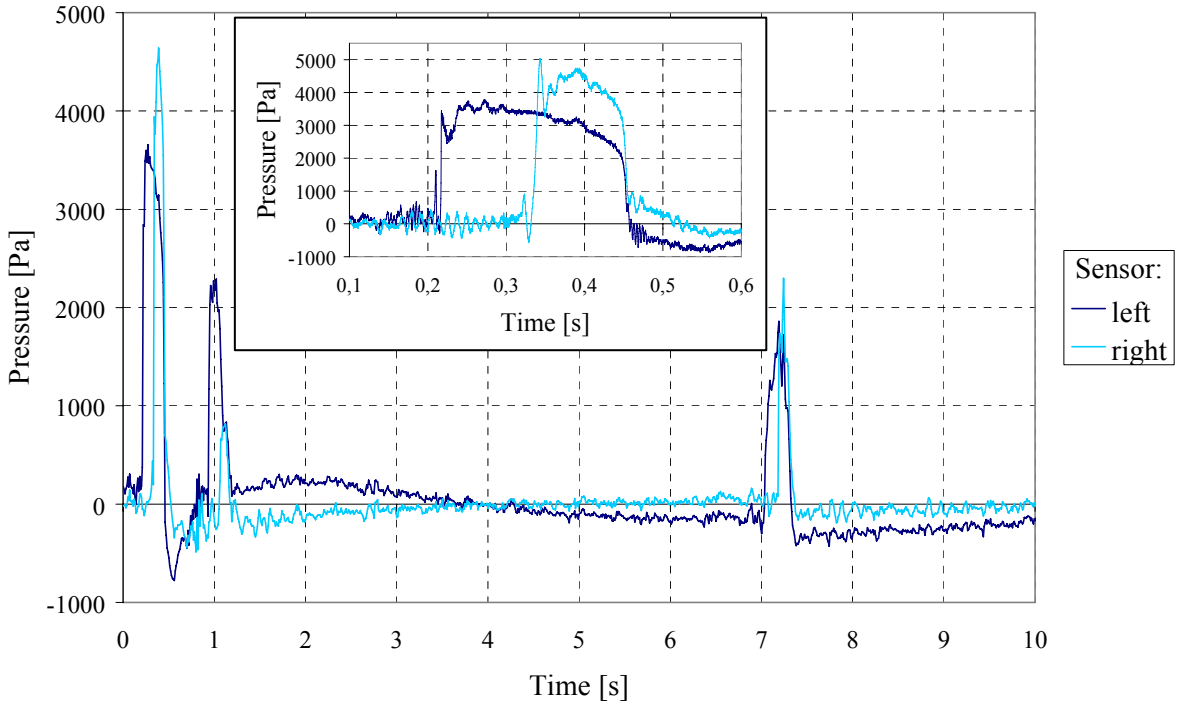

Fig. 3.10: Typical pressure measurement by slug flow and zoom in on the first pressure increase

b. Comparison with the calculation

Because the slug also closes the channel cross-section in the calculation, an area with high pressure is created after the slug (see Fig. 3.11).

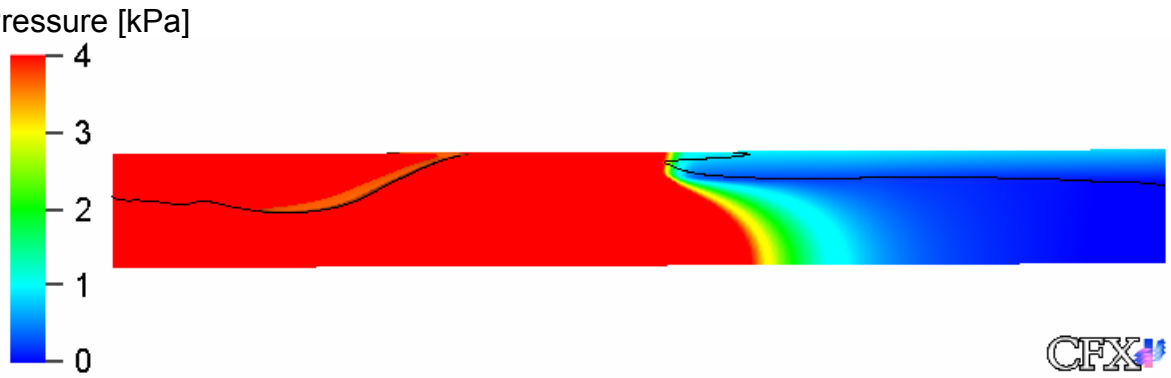

Fig. 3.11: Calculated pressure field and interface at t = 0.95 s

Fig. 3.12 shows the comparison of the time-dependant pressure at both sensor positions for the experiment and the CFD calculation. Since it was not possible to simulate the first slug, there is no pressure peak in the calculation that corresponds to the first experimentally observed peak. During the travelling of the second slug, the pressure at the first sensor position increases later in the calculation than in the experiment, which is due to the lower velocities in the acceleration phase. At the second sensor position, the pressure increase is simultaneous. Then, the pressure decreases earlier in the calculation than in the experiment, i.e. the calculated slug

becomes faster than in reality. This is in agreement with the remarks made on the slug position diagram (see paragraph 3.5.2 and Fig. 3.9).

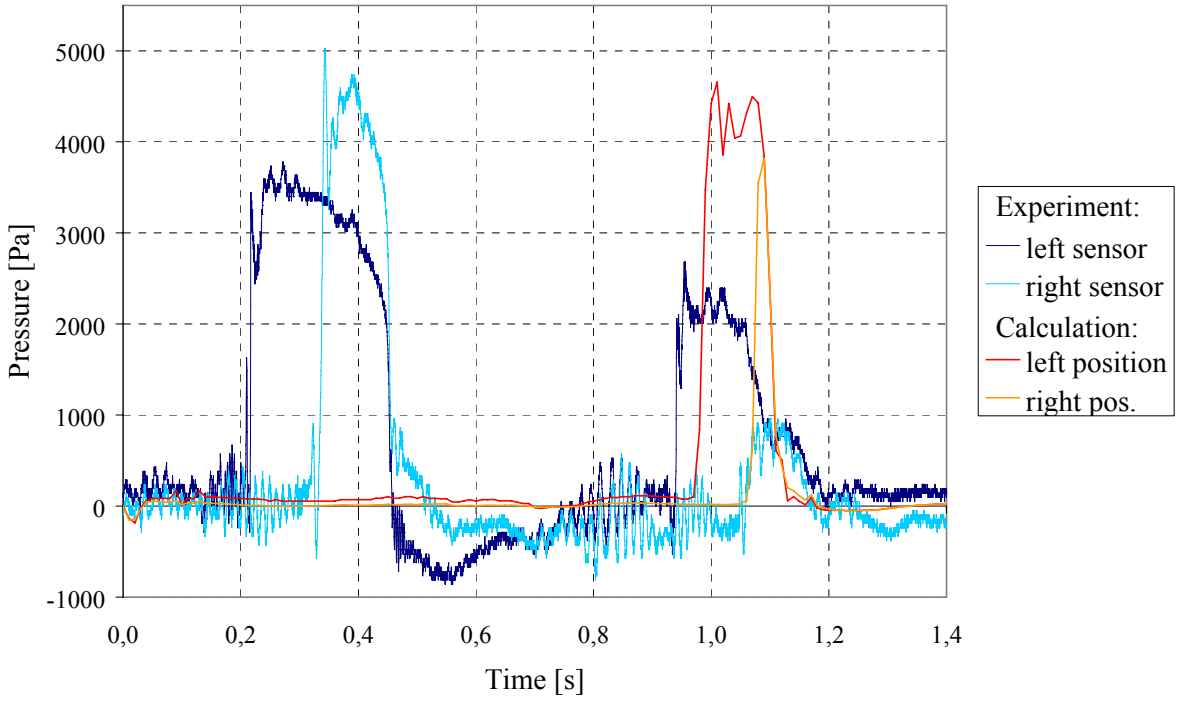

Fig. 3.12: Transient pressure at the left and right sensor positions for experiment and *ANSYS CFX* calculation

Furthermore, for the recalculated slug, the pressure peak value is higher in the calculation (4.4 kPa) than in the measurement (2.3 kPa), whereas the peak value of the first slug observed in the experiment reaches between 3.6 and 5.0 kPa (respectively at the first and second sensor positions), which is in much better agreement with the calculated value.

This difference of the experimental pressure peak value is due to the fact, that the boundary conditions for the second slug are already influenced by the first slug, which has cleared a certain amount of water from the channel before. The lower pressure peak of the second slug can be explained by the smaller amount of water to be driven by the air pressure. Furthermore, the effective free area on top of the slug where air flows is bigger. This effect is missing in the calculation, since the first slug was not reproduced.

3.5.4 Particle Image Velocimetry (PIV) of a slug

To show the inner structure of the velocity field of a slug, a PIV-system was used. The laser-light sheet was focused to the vertical mid-plane of the test section. The PIV-camera was directed from the side to the upper part of the duct, in the region of the first pressure sensor (z_f = 1.45 m). The limited size of the observation area (140 x 105 mm²) did not allow to cover the entire height of the channel of 250 mm.

Fig. 3.13 shows a PIV-picture of a slug with the calculated velocity field. The slug propagation velocity was 3.8 m/s (in the same region as chosen in paragraph 3.5.2),

which is similar to the slug velocity of the recalculated slug. The vector colour shows that the entrained air flow on top of the slug accelerates the water to absolute local velocities of about 6 m/s.

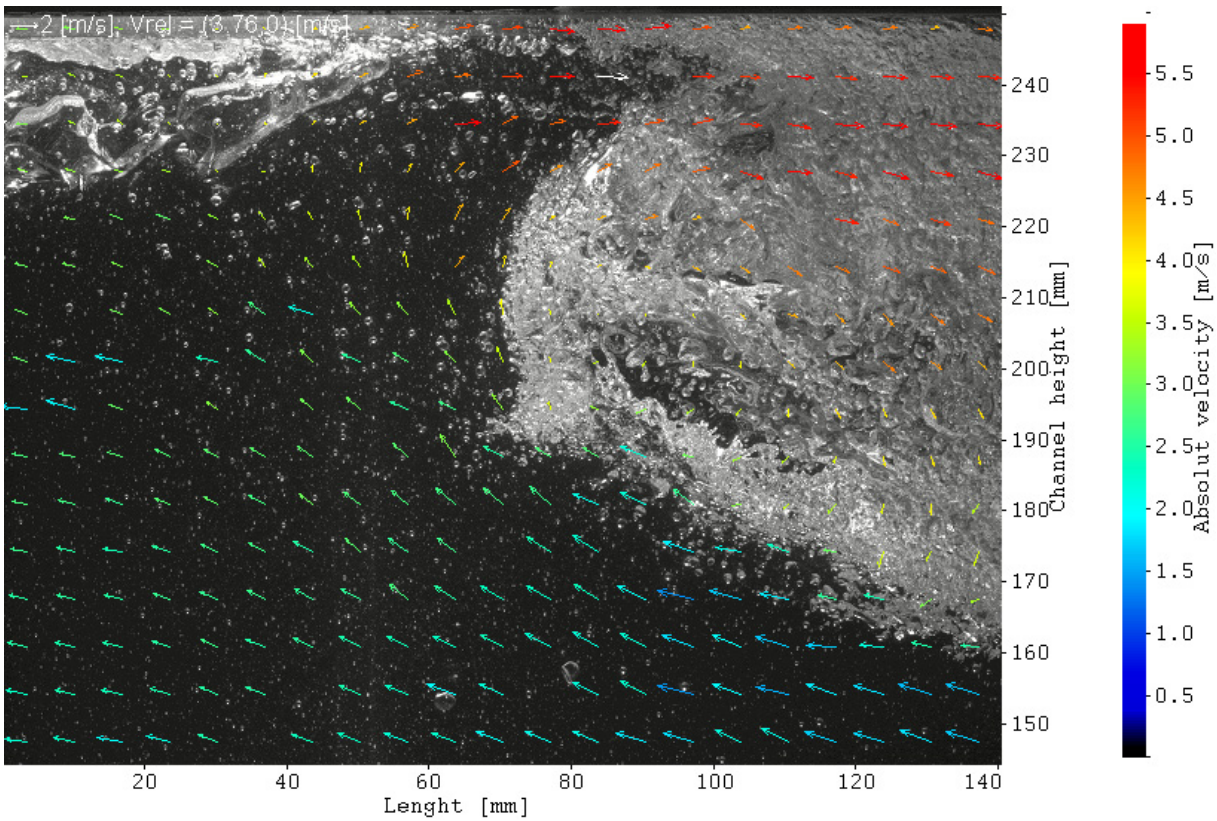

Fig. 3.13: Velocity field of the secondary flow inside of a slug (the vector colour shows the absolute velocity; the vector length and direction show the relative velocity after subtracting the propagation velocity of the slug)

The vector direction and length show the relative velocities after subtraction of the propagation velocity of the slug itself. It reveals the secondary flow pattern inside of the slug. At the slug front, the water steams upwards. On top, it is accelerated in direction of the slug movement and becomes faster than the slug itself. Due to gravity, the portions that roll over fall down again. In this way, the roll-over vortex structure is formed. On the left side of the image, water seems to flow against the main flow direction. This is true in the coordinate system of the slug, since this water flow is slower than the slug. In reality it flows in the right direction, of course.

3.6 Conclusions

This preliminary study shows that the slug flow regime can be qualitatively reproduced with CFD. In order to perform reasonable quantitative comparisons, the experimental boundary conditions at the inlet have to be constant and well defined. Because of the separator at the test-section inlet, important inlet parameters such as water level and velocity profiles cannot be controlled properly and are not stationary in the present facility. Therefore, detailed investigations require improved inlet geometry. This was realised in a new test facility, which is described in section 4.

4. CFD model for a self-generation of slug flow

4.1 The Horizontal Air/Water Channel (HAWAC)

The **H**orizontal **A**ir/**Wa**ter **C**hannel (HAWAC) (Fig. 4.1) is devoted to co-current flow experiments. A special inlet device provides defined inlet boundary conditions by a separate injection of water and air into the test-section. The cross-section of this channel is smaller than the previous one (described in section 3): its dimensions are 100 x 30 mm² (height x width). Thus it fits the field of view of the PIV-system and makes it possible to cover a wider range of superficial velocities. The test-section is about 8 m long, and therefore the length-to-height ratio *L/H* is 80. Alternatively, related to the hydraulic diameter, the dimensionless length of the channel is L/D_h = 173.

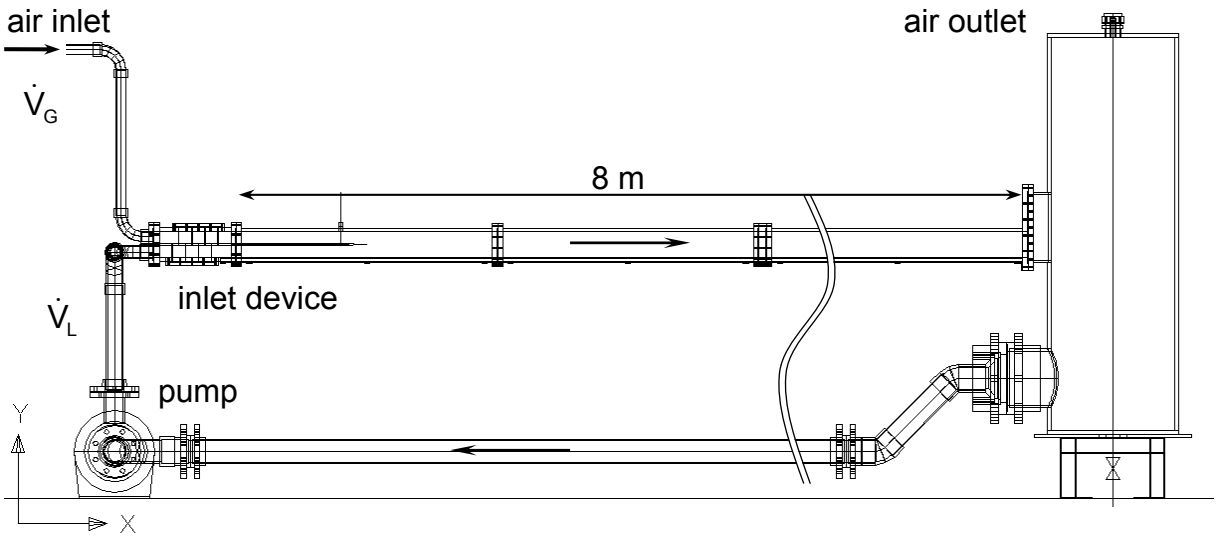

Fig. 4.1: Schematic view of the Horizontal Air/Water Channel (HAWAC)

The inlet device (Fig. 4.2) is designed for a separate injection of water and air into the channel. The air flows through the upper part and the water through the lower part of this device. Because the inlet geometry produces a lot of perturbations in the flow (bends, transition from pipes to rectangular cross-section), 4 wire mesh filters are mounted in each part of the inlet device. The filters are made of stainless steel wires with a diameter of 0.63 mm and have a mesh size of 1.06 mm. They aim at providing homogenous velocity profiles at the test-section inlet. Moreover, the filters produce a pressure drop that attenuate the effect of the pressure surge created by slug flow on the fluid supply systems.

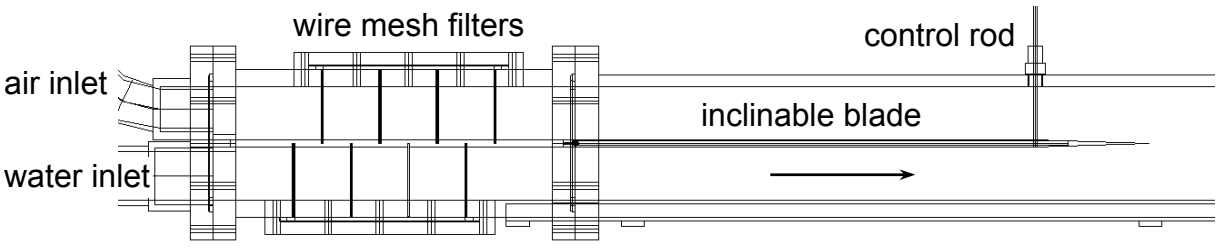

Fig. 4.2: The HAWAC inlet device

Air and water come in contact at the final edge of a 500 mm long blade that divides both phases downstream of the filter segment. The free inlet cross-section for each phase can be controlled by inclining this blade up and down. Both, filters and inclinable blade, provide well-defined inlet boundary conditions for the CFD model and therefore offer very good validation possibilities.

The water flow rate is measured with a paddle-wheel flow transmitter and adjusted via the frequency inverter of the pump motor. The air flow rate is measured and controlled with the thermal mass flow meters of the TOPFLOW-facility. These are mounted in parallel in order to ensure a high precision over a large measuring range. The flow rates are measured with an accuracy of ±0,2 l/s for the water and ±1,5% for the air. The maximum superficial velocities achieved in the test-section are 2 m/s for the water and 8 m/s for the air. Optical measurements were performed with a high-speed video camera.

4.2 Influence of the inlet blade position on the two-phase flow generation

The adjustable inclination of the inlet blade separating the phases allows to influence the generation of the two-phase flow regime. The first contact between gas and liquid can be modified with the blade position: if the velocities at the end of the blade are similar, a smooth come together will be managed, else a perturbation can be introduced in the channel. For example, observations have shown that the inlet length needed for slug generation can vary from 0.5 to 3 m just by changing the blade inclination from an opening ration of 20/80 (air/water) to 80/20. Nevertheless, and despite a short channel length, the flow regime established at the end of the channel is not significantly affected by the plate inclination.

Furthermore, at high water flow rates, especially when the inlet blade is inclined down, a hydraulic jump can be realised in the test-section. As shown in Fig. 4.3, the hydraulic jump is the turbulent transition zone between super- and subcritical flow. In the supercritical region, the flow is always stratified, whereas after the hydraulic jump (i.e in the subcritical region) the typical two-phase flow regimes were observed (e.g. elongated bubble flow, slug flow). The position of the hydraulic jump in the channel depends on both flow rates and on the inlet blade inclination. When a hydraulic jump is formed, its position strongly influences the inlet length needed for the generation of slug flow.

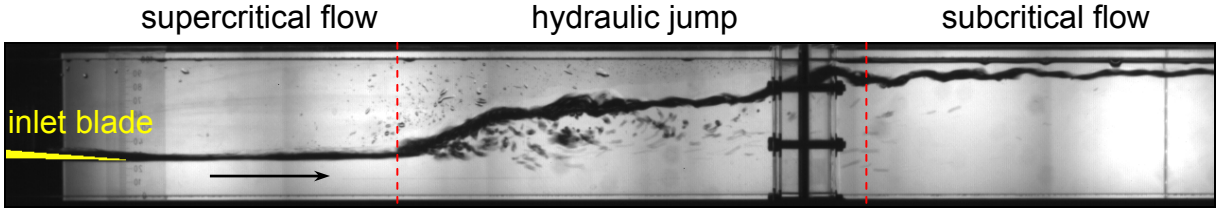

Fig. 4.3: Hydraulic jump in the test-section (j_L = 0.37 m/s; j_G = 0.10 m/s, inlet blade = 26 mm)

It was observed that the position of the inlet blade not always defines the water level at the channel inlet. For example when the inlet blade is inclined upwards and the water flow rate is very low, the water flow separates from the lower surface of the blade. In this case, the initial water level is lower than the height of the outlet edge of

the blade. To create proper inlet boundary conditions at these flow rates, the blade has to be inclined down.

4.3 Flow pattern map of the HAWAC

A flow pattern map (Fig. 4.4) was arranged on the basis of visual observations of the flow structure at different combinations of the gas and liquid superficial velocities. The observed flow patterns are:

- 1 stratified flow
- 2 wavy flow
- 3 elongated bubble flow
- 4 slug flow

Further, sub-categories were defined to consider the slug generation frequency and the appearance of elongated bubbles:

- a sporadic (transition regime)
- b periodic, but only one type of structure (either slug or elongated bubble)
- c periodic and several types of structure simultaneously

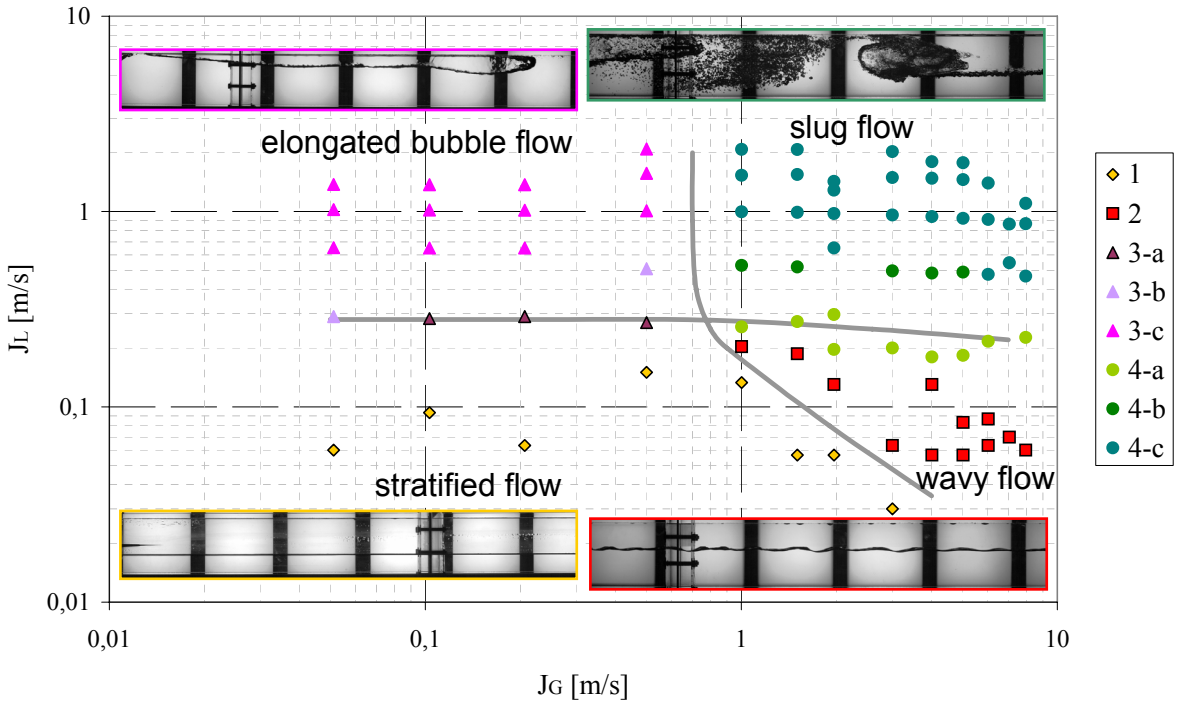

Fig. 4.4: Flow pattern map for the rectangular channel (inlet blade in horizontal position)

In the flow map, some transitions are different from those found by Mandhane (1974) and Baker (1954). Especially the transitions from stratified to elongated bubble flow and from wavy to slug flow were observed at higher liquid superficial velocities than in the literature. This can be attributed to the shorter channel length and would indicate that the flow regime is not fully established at the end of the test-section. Another source of discrepancy could be the cross-section geometry: the results from Mandhane are based on pipe measurements, whereas ours were performed in a channel with rectangular cross-section.

4.4 CFD model of the duct, turbulence modelling in the interfacial area and boundary conditions

The second channel with rectangular cross-section was modelled using *ANSYS CFX*. The model dimensions are 4000 x 100 x 30 mm³ (length x height x width), which corresponds only to the first half of the test-section (Fig. 4.5-a). The grid consists of $6x10^5$ hexahedral elements.

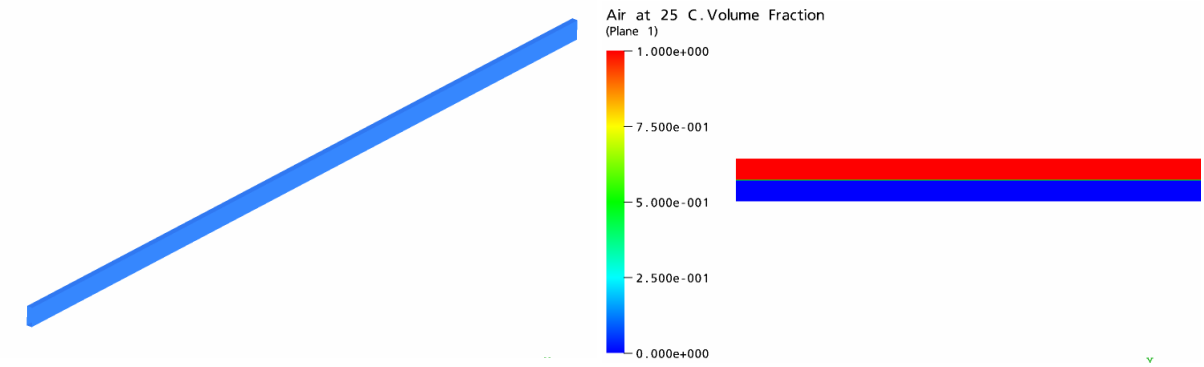

a) Fluid domain (channel) b) Air volume fraction, initial state (Zoom)

Fig. 4.5: Model and initial conditions of the mass fractions

The slug flow experiment at a superficial water velocity of 1.0 m/s and a superficial air velocity of 5.0 m/s was chosen for the CFD calculations. In the experiment, the inlet blade was in horizontal position. Accordingly, the model inlet was divided into two parts: in the lower 50% of the inlet cross-section, water was injected and in the upper 50% air. An initial water level of y_0 = 50 mm was assumed for the entire model length (Fig. 4.5-b).

In the simulation, both phases have been treated as isothermal and incompressible, at 25°C and at a reference pressure of 1 bar. A hydrostatic pressure was assumed for the liquid phase. Buoyancy effects between the two phases are taken into account by the directed gravity term. At the inlet, the turbulence properties were set using the “Medium intensity and Eddy viscosity ratio” option of the flow solver. This is equivalent to a turbulence intensity of 5% in both phases. The inner surface of the channel walls has been defined as hydraulically smooth with a non-slip boundary condition applied to both gaseous and liquid phases. The channel outlet was modelled with a pressure controlled outlet boundary condition.

As the goal of the CFD calculation was to induce surface instabilities, which are later generating waves and slugs, the interfacial momentum exchange and also the turbulence parameters had to be modelled correctly. Without any special treatment of the free surface, the high velocity gradients at the free surface, especially in the gaseous phase, generate too high turbulence throughout the two-phase flow when using the differential eddy viscosity models like the *k-ε* or the *k-ω* model (*ANSYS CFX*, 2006). Therefore, certain damping of turbulence is necessary in the interfacial area because the mesh is too coarse to resolve the velocity gradient in the gas at the interface. On the gas side of the smooth free surface, this damping should be similar to that used near a solid wall. Moreover, on the liquid side the advanced model should take the anisotropy between the normal and the tangential Reynolds stresses into account. A simple symmetric damping procedure provides for the solid wall-like damping of turbulence in both gas and liquid phases. Therefore, a damping of

turbulent diffusion at the interface was applied in this calculation by an appropriate source term in the ω-equation:

$$A \cdot \Delta y \cdot \beta \cdot \rho_i \cdot \left(B \cdot \frac{6 \cdot \mu_i}{\beta \cdot \rho_i \cdot \Delta n^2} \right)^2 \tag{4.1}$$

where A the interface area density, Δn is the typical grid cell size across the interface, ρ_i and μ_i are the density and viscosity of the phase i. Further, the model parameter B should have a value of 100.

The parallel transient calculation of 5.0 s of simulation time on 4 processors last 4 days. A high-resolution discretization scheme was used. For time integration, the fully implicit second order backward Euler method was applied with a constant time step of dt = 0.001 s and a maximum of 15 coefficient loops. A convergence in terms of the RMS values of the residuals to be less then 10^{-4} could be assured most of the time.

4.5 Results

In the following picture sequences (Fig. 4.6 and Fig. 4.7) a comparison is presented between CFD calculation and experiment: the calculated phase distribution is visualized and comparable camera frames are shown. In both cases, a slug is generated. The sequences show that the qualitative behaviour of the creation and propagation of the slug is similar in the experiment and in the calculation. In the CFD calculation, the slug develops at approximately t = 1.30 s, induced by instabilities.

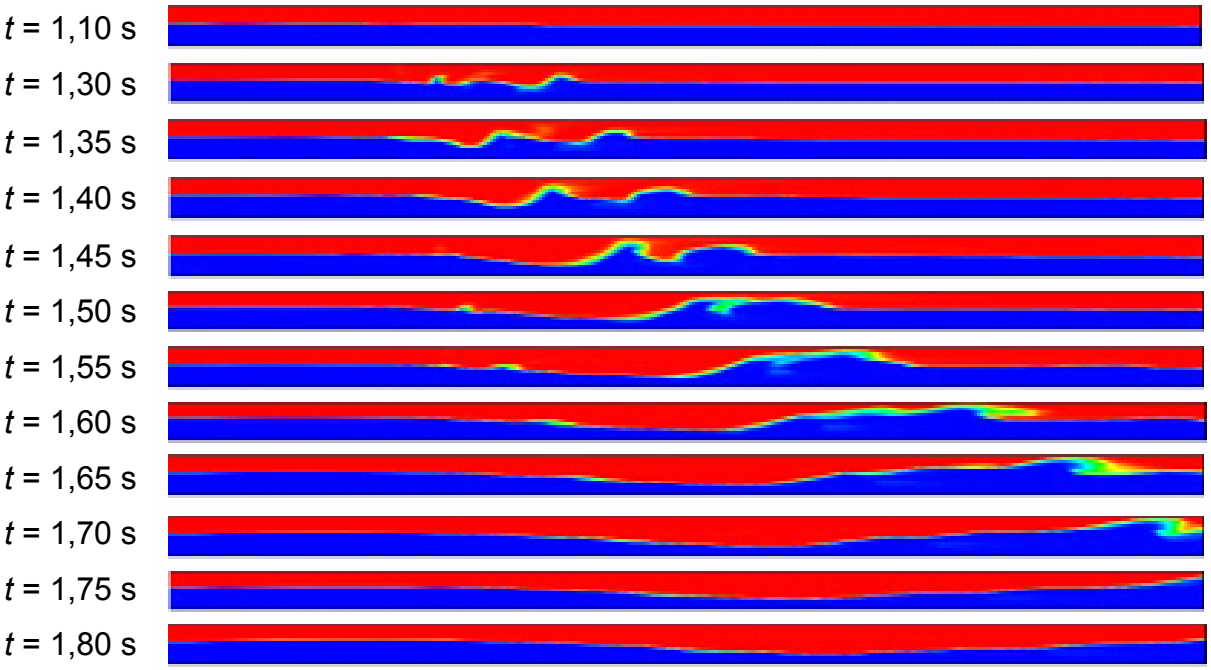

Fig. 4.6: Calculated picture sequence at J_L = 1.0 m/s and J_G = 5.0 m/s (depicted part of the channel: 1.4 to 4 m after the inlet)

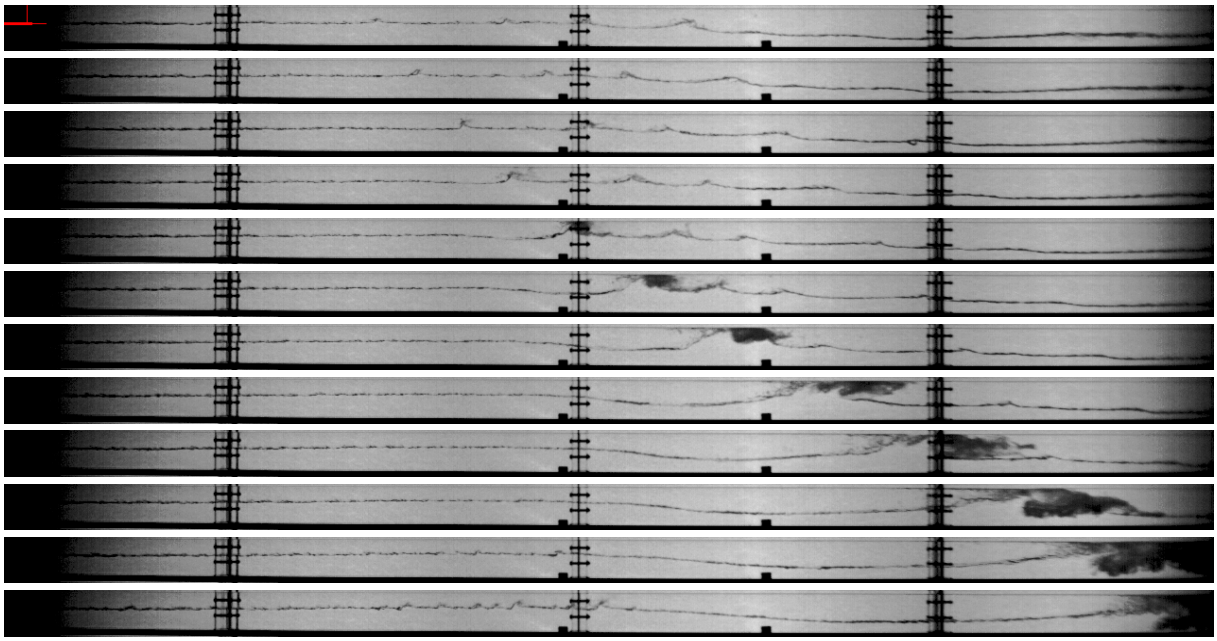

Fig. 4.7: Measured picture sequence at J_L = 1.0 m/s and J_G = 5.0 m/s with Δt = 50 ms (depicted part of the channel: 0 to 3.2 m after the inlet)

The single effects leading to slug flow that can be simulated are shown in details in Fig. 4.8. These phenomena are:

- Instabilities and small waves are generated by the interfacial momentum transfer randomly (Fig. 4.8-a). As a result bigger waves are generated.
- The waves can have different velocities and can merge together (Fig. 4.8-b and c).
- Bigger waves roll over (Fig. 4.8-c) and can close the channel cross-section (Fig. 4.8-d).

The needed entrance length for slug generation was defined as the length between the inlet and there a wave closes nearly the entire cross-section for the first time. This was observed at about 1.5 m in the experiment and 2.5 m in the calculation.

In contrast to the measurement, the stratified flow after the slug calculated with *ANSYS CFX* is too smooth which defers the generation of the next slug. Since the slug cleared an important amount of water from the channel, the next slug appears after the channel is slowly filled up again by the transport of liquid from the inlet. This process takes approximately 1.5 s. In the experiment, small waves are generated immediately after the slug and create the next one within 0.3 to maximum 0.7 s. Sources of instabilities are here the high air velocity but also the pressure surge created by the slugs, particularly when they leave the channel. This effect has not been proper simulated since just the half of the channel was modelled. Therefore, the slug frequency cannot be compared at this stage of the simulation.

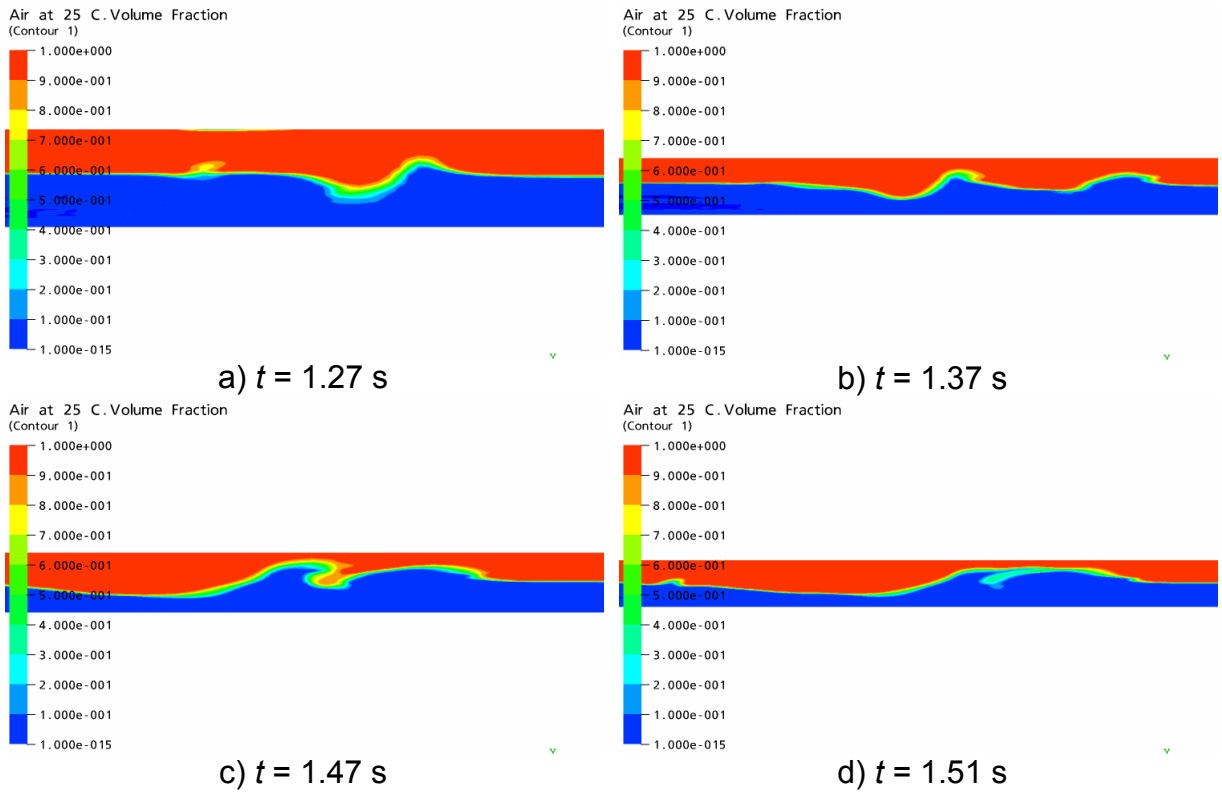

Fig. 4.8. Details of the slug generation calculated with *ANSYS CFX* at different simulation time

5. Hot-leg model pre-test calculations

5.1 Background: the reflux condenser mode and the counter-current flow limitation

In the event of a loss-of-coolant-accident (LOCA) in a pressurised water reactor (PWR), emergency strategies have to be mapped out, in order to guarantee a safe removal of heat from the reactor core, also in case of component breakdown. During a small break LOCA with failure of the high pressure emergency core cooling system (ECC) and of the main feed pumps, a natural circulation starts in the primary circuit. This allows the heat removal, also if steam is generated in the reactor core due to the depressurisation of the primary circuit. But if further the water level in the reactor pressure vessel (RPV) falls below the hot-leg inlet, only steam will flow to the steam generator. Therefore the natural circulation breaks down and switches to the reflux condenser mode.

In the reflux condenser mode, the steam coming from the RPV condensates in the vertical U-tubes of the steam generator. In each half of the steam generator, the condensate flows down the tube in which it has been formed. Therefore, about one half of the condensate flows as usual over the pump to the downcomer, whereas the other half flows over the hot-leg back to the upper plenum. In the hot-leg, the condensate have to flow in counter-current to the steam (Fig. 5.1).

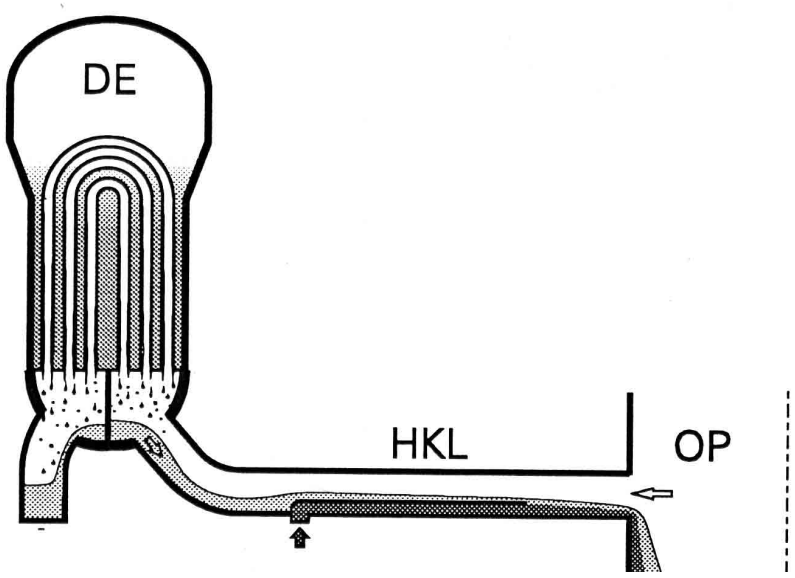

Fig. 5.1: Schematic view of the flow in the hot-leg and steam generator during reflux condenser mode (GRS, 1993)

The horizontal stratified counter-current flow of condensate and steam is only stable for a certain range of flow rates. If the steam flow increases too much, the condensate is clogged in the hot-leg. This is the begin of the counter-current flow limitation (CCFL): the liquid is carried over by the steam and partially entrained in opposite direction to the steam generator (Fig. 5.2). As a consequence, the hot-leg and steam generator are flood, which decreases the water level in the RPV and reduces the core cooling. In case of an additional increase of the steam flow, the

condensate is completely blocked and the cooling of the reactor core from the hot-leg is impossible.

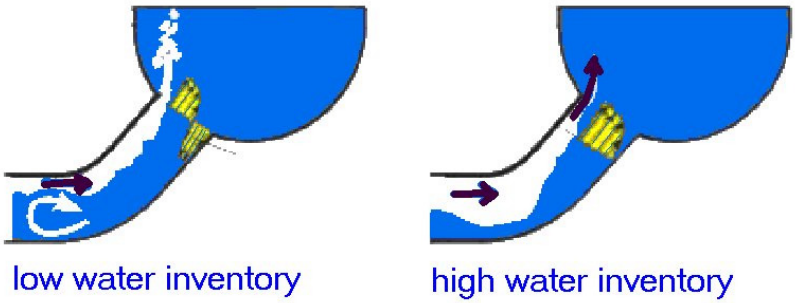

Fig. 5.2: Possible flow phenomena in the hot-leg bend during CCFL (GRS, 1993)

5.2 The hot-leg model in the pressure chamber of the TOPFLOW-facility

For the experimental investigation of stratified two-phase flow in a complex geometry, the “hot-leg model” was constructed at *Forschungszentrum Dresden-Rossendorf*. The hot-leg model is built in the pressure chamber of the TOPFLOW facility, which is used to perform experiments with steam/water at pressures up to 50 bars and temperatures up to 264°C, but under pressure equilibrium with the chamber inside (Fig. 5.3). A special heat exchanger condenses the exhaust steam from the test section in the chamber. Its cold end is permanently connected to the inner atmosphere of the chamber in order to guarantee full pressure equilibrium at all times (Fig. 5.4). Therefore, the test section does not have to support overpressures and can be designed with thin materials.

Fig. 5.3: The pressure chamber and the test-section components

In the hot-leg experiment, the test-section is a steal frame with glass side walls for high-speed video observations. Its outlines represent a 1:3 hot-leg model of the German *Konvoi*-reactor and corresponds to a channel height of 250 mm (straight part of the hot-leg). The experiments focus on the flow regimes observed in the region of the elbow and of the steam generator inlet chamber during counter-current flow limitation.

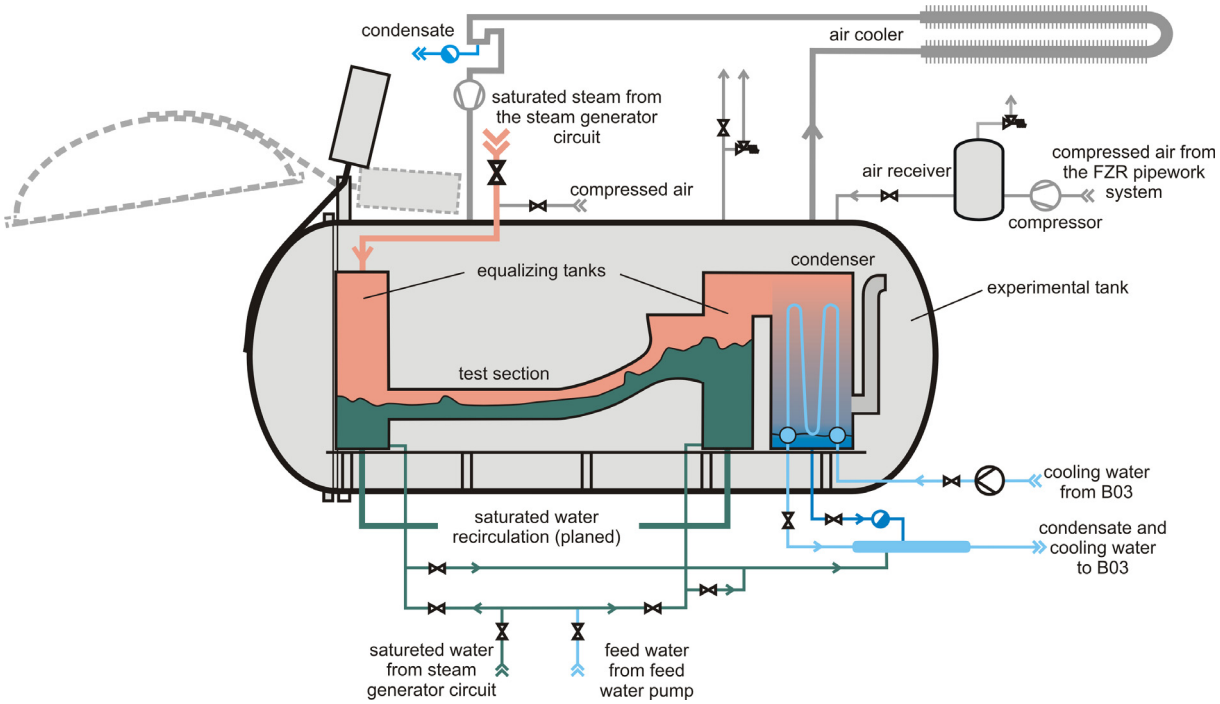

Fig. 5.4: Scheme of the pressure chamber setup

Because of technical problems with the pressure chamber of the TOPFLOW facility, no experiments could be performed in the frame of the current project. However CFD pre-test calculations were done to show the possibility of slug flow simulation in the geometry of the hot-leg model in a steam/water flow.

5.3 CFD model of the hot-leg

5.3.1 Modelled scenario

The aim of the numerical simulation is the investigation of the feasibility of numerical prediction of stratified two-phase flow with *ANSYS CFX* in a real geometry and at relevant parameters for nuclear reactor safety.

For the present CFD calculation, a hypothetical scenario was selected with a typical stratified flow in the hot-leg. At the beginning of the simulation, the primary circuit is filled with a constant coolant level at approximately 3/4 of the main lines diameter. Nevertheless, steam is produced in the RPV and is streaming through the remaining cross-section towards the hot-leg into the steam generator. The assumed pressure is 50 bar and the steam is at saturation conditions. The test should show the resulting surface behaviour of the interphase, for example the formation of waves and/or slugs in the hot-leg.

5.3.2 Geometry and grid generation

Due to very high numerical efforts of transient slug flow simulations, the modelling of the complete test-section including the separators is not feasible. In order to keep computational time within acceptable limits, in a first approach only the horizontal test-section was modelled (Fig. 5.5). The grid was created with CFX-MESHBUILD and transferred to CFX-PRE. It consists of 1.4 x 10^5 hexahedral elements, which reduces the computational time and improves the quality of the mesh compared to tetrahedrons.

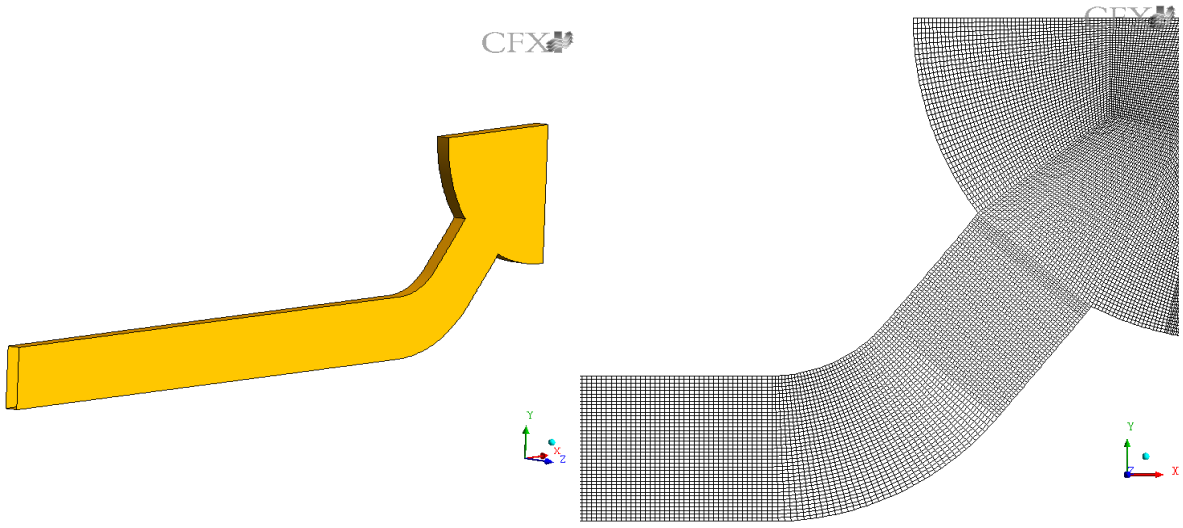

a) simplified model: hot-leg and steam generator inlet chamber

b) grid: zoom on the bend and steam generator inlet chamber

Fig. 5.5: CFD model of the hot-leg test-section

5.3.3 Boundary conditions

Corresponding to the described scenario, the initial water level in the horizontal part of the hot-leg was set to y_0 = 0.194 m over the entire free surface. A hydrostatic pressure was assumed for the liquid phase.

The inlet of the CFD model is the vertical cross-section of the horizontal part of the hot-leg, which is opened to the RPV in the original primary circuit. Following inlet boundary conditions were chosen for the calculation and were kept constant during the simulation time:

- height of the steam inlet: $0.194 \leq y \leq 0.25$ m
- steam superficial velocity: j_G = 3.0 m/s (i.e. mass flow rate: 0.213 kg/s)
- water superficial velocity: j_L = 0.0 m/s

The inlet turbulence properties have been set using the “Medium intensity and Eddy viscosity ratio” option of the flow solver, which is equivalent to a turbulence intensity of 5% in both phases.

A pressure controlled outlet boundary condition was applied to the vertical cross-section of the steam generator inlet chamber, which corresponds to the connection to the separator in the experiment. The inner surface of the channel walls was defined as hydraulically smooth with a non-slip boundary condition applied to both gaseous and liquid phases.

5.3.4 Fluid properties

The gaseous phase is steam and the liquid phase is water, both saturated at 263.9°C and at a reference pressure of 50 bar. The fluid densities and viscosities are taken from Table 1 (values are highlighted for 50 bar). The phases have been treated as isothermal and incompressible. Buoyancy effects between the two phases are taken into account by the directed gravity term.

Table 1: Water and steam properties

pressure	**saturation temperature**	**density [kg/m³]**		**kinematic viscosity [m²/s]**	
[bar]	**[°C]**	**water**	**steam**	**water**	**steam**
7.5	167.76	899.7	3.91	$1.80 \cdot 10^{-7}$	$3.73 \cdot 10^{-6}$
10.0	179.89	887.1	5.15	$1.69 \cdot 10^{-7}$	$2.92 \cdot 10^{-6}$
30.0	233.86	821.9	15.00	$1.39 \cdot 10^{-7}$	$1.13 \cdot 10^{-6}$
50.0	**263.94**	**777.4**	**25.35**	$\mathbf{1.29 \cdot 10^{-7}}$	$\mathbf{7.11 \cdot 10^{-7}}$

5.3.5 Discretization schemes, time step and convergence

A high resolution discretization scheme was used. For time integration, the fully implicit second order backward Euler method was applied with a constant time step of $\Delta t = 0.001$ s and a maximum of 15 coefficient loops. A convergence in terms of the RMS values of the residuals to be less then 10^{-4} could be assured most of the time.

5.4 Results

The results of the transient CFD-calculation are shown in image sequences of the phase distribution (Fig. 5.6) and of the steam velocity field (Fig. 5.7). After about 0.2 s of simulation time, the water level begins to incline upwards in direction of the steam generator. This is the result of the interfacial momentum exchange between the steam and the stagnant water. At the water surface, small waves are generated randomly in the horizontal part of the hot-leg and propagate in direction of the bend.

The velocity fields show that the waves crest constrict the steam cross-section and causes an acceleration of the steam velocity, especially in the bended region of the hot-leg model (Fig. 5.7). Moreover, swirls are formed downstream of the biggest waves (e.g. at 0.27 s).

From 1,52 s, slugs are generated and transport liquid over the steam generator bottom to the outlet. The slugs cause a water loss in the horizontal part of the channel and the water level is decreasing. As a consequence, the cross-section for the steam is widening and the slugging finishes. From about t = 4,5 s, the flow regime in the hot-leg is again wavy flow.

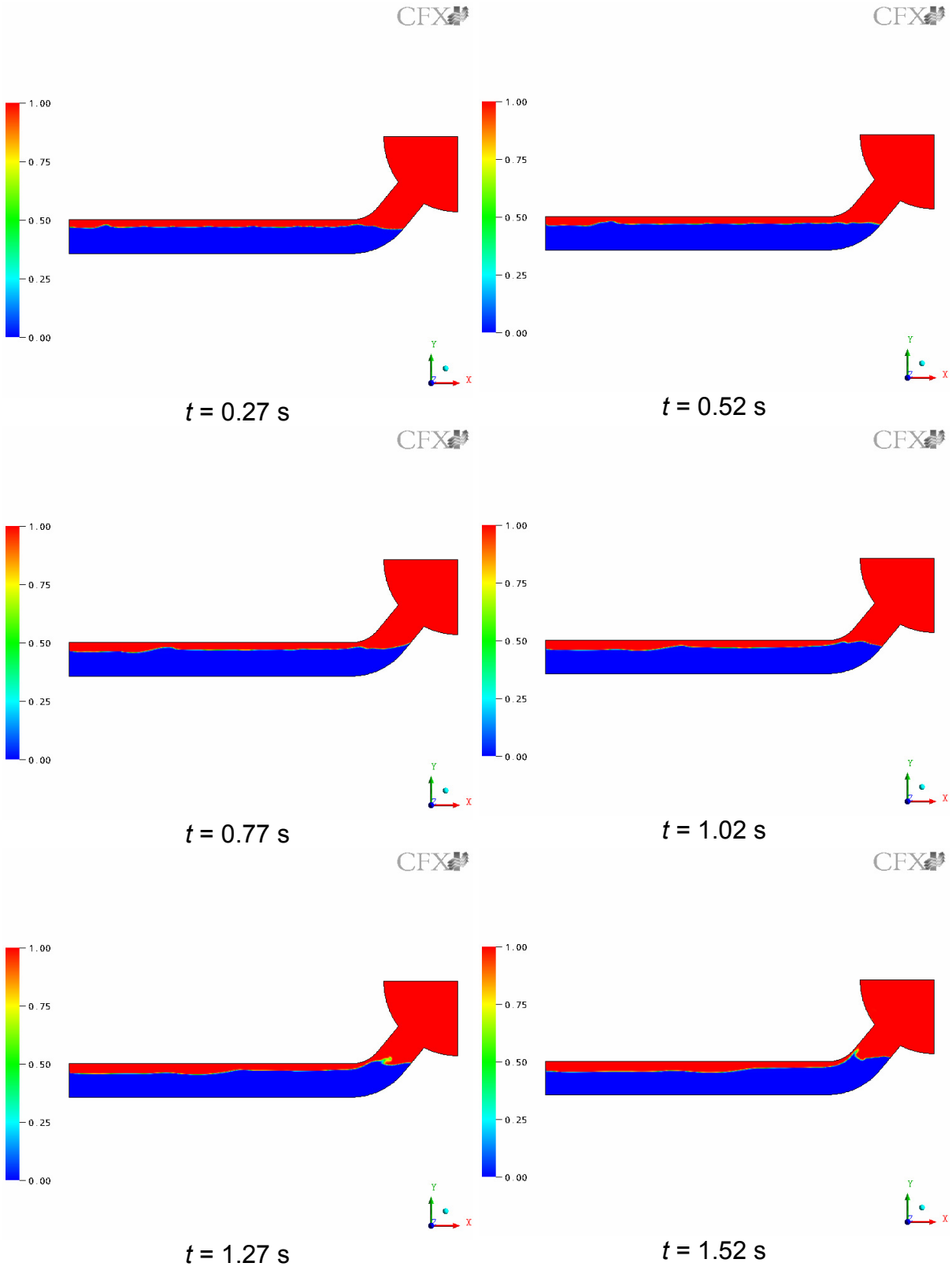

Fig. 5.6: Steam volume fraction in the hot-leg model over the time, calculated with *ANSYS CFX*

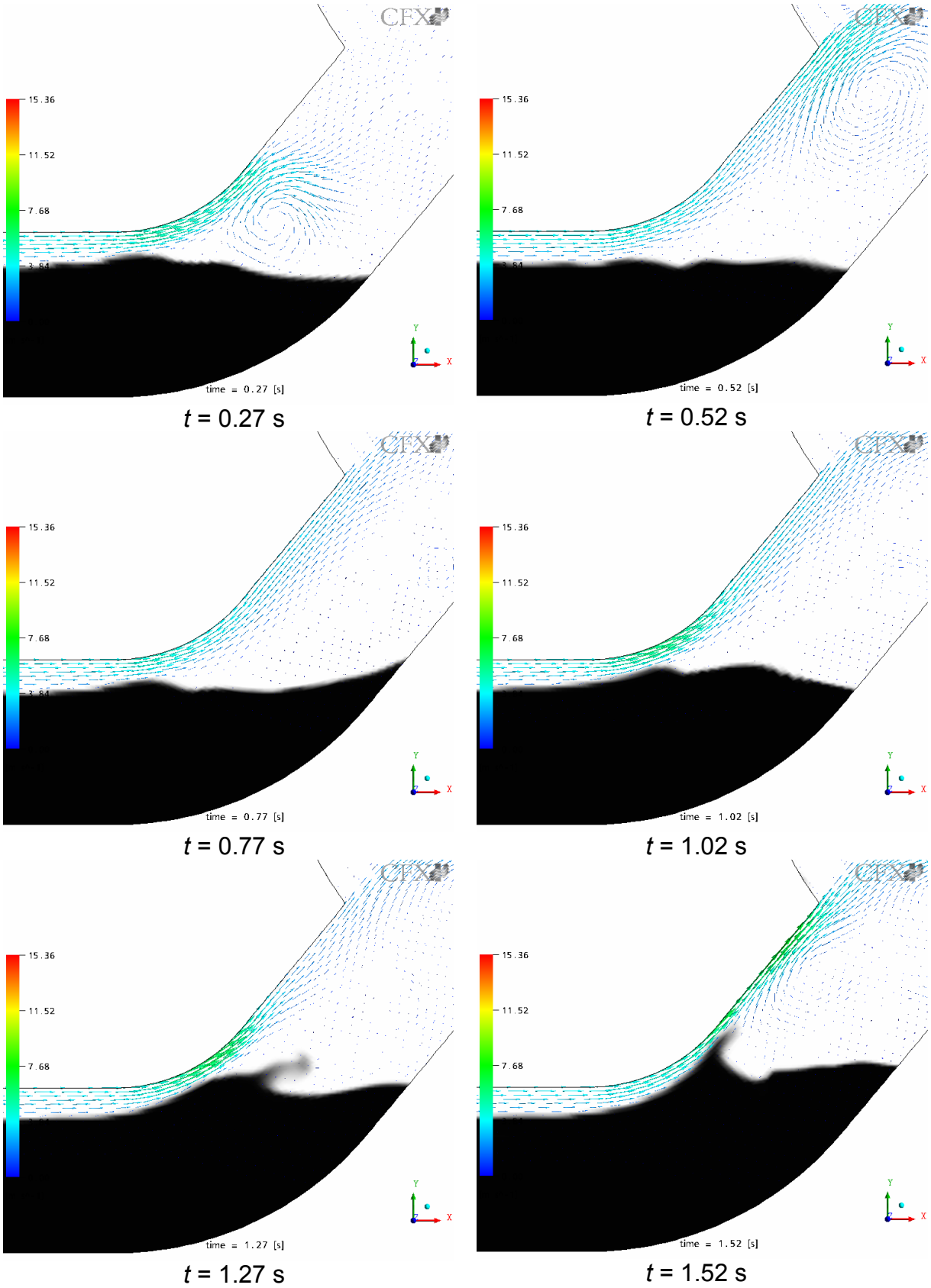

Fig. 5.7: Steam velocity distribution in the bended region of the hot-leg model over the time, calculated with *ANSYS CFX* (water: black labelled)

6. Summary and conclusions

For the investigation of an air/water slug flow, two horizontal channels with rectangular cross-section were built at *Forschungszentrum Dresden-Rossendorf* (FZD). In the first channel with a separator at the inlet, optical measurements were performed with a high-speed video camera and were complemented by simultaneous dynamic pressure measurements. By an interface capture method, the water level history can be extracted from the image sequences. Furthermore, the velocity field of a slug was measured using Particle Image Velocimetry (PIV). It reveals the inner flow circulation of the slug, around the point there the slug is rolling over. A CFD simulation of stratified co-current flow was performed using the code *ANSYS CFX* (version 5.7) applying the two-fluid model with the free surface option. No explicit interface tracking methods (e.g. VOF or Level Sets methods) were used. Slug flow was successfully simulated with a transient simulation, using a time-dependent inlet water level from the experimental data.

In the HAWAC test facility, a special inlet device provides well defined as well as variable boundary conditions, which allow very good CFD-code validation possibilities. A flow pattern map was arranged and shows the potential of the facility. A picture sequence recorded during slug flow was compared with the equivalent CFD simulation made with the code *ANSYS CFX*. The two-fluid model was applied with a special free surface treatment. Due to an interfacial momentum transfer, it was possible to generate slugs based on instabilities. The behaviour of slug generation and propagation at the experimental setup was qualitatively reproduced, while deviations require a continuation of the work. The creation of small instabilities due to pressure surge or an increase of interfacial momentum should be analysed in the future. Furthermore, pressure and velocity measurements should be performed in the HAWAC facility to allow quantitative comparisons, also at other superficial velocities.

CFD pre-test calculations were done to show the possibility of slug flow generation in a real geometry and at relevant parameters for nuclear reactor safety. The simulation was performed on a flat model representing the hot-leg of the German *Konvoi*-reactor at the scale of 1:3. The fluids were water and steam at a pressure of 50 bar and the corresponding saturation temperature of 263.9°C. The results of the CFD-calculation show first an upwards inclination of the stagnant water in direction of the steam generator, driven by the momentum exchange from the injected steam. Further, waves are generated randomly in the horizontal part of the hot-leg and grow to slugs in the region of the bend.

7. References

ANSYS CFX (2006). User Manual. ANSYS Inc.

Anglart, H., and Podowski, M. Z. (2002). Fluid mechanics of Taylor bubbles and slug flows in vertical channels. Nuclear science and engineering, 140, 165-171.

Baker, O. (1954). Simultaneous flow of oil and gas. Oil & Gas Journal, 53, 184-195.

Cook, M., and Behnia, M. (2001). Bubble motion during inclined intermittent flow. Int. J. of Heat and Fluid Flow, 22, 543-551.

Frank, T. (2003). Numerical simulations of multiphase flows using CFX-5. CFX Users conference, Garmisch-Partenkirchen, Germany.

Hope, C. B. (1990). The development of a water soluble photocromic dye tracing technique and its application to two-phase flow. PhD thesis, Imperial College of Science, Technology and Medicine, London.

Ishii, M. (1990). Two-fluid model for two-phase flow. Multiphase Science and Technology, 5, Edited by G. F. Hewitt, J. M. Delhaye, N. Zuber, Hemisphere Publishing Corporation, 1-64.

Issa, R. I., and Tang, I. F. (1990). Modelling of vertical gas-liquid slug flow in pipes. Proc. Symp. On Advances in Gas-Liquid flows, Dallas.

Lun, I., Calay, R. K., and Holdo, A. E. (1996). Modelling two-phase flows using CFD. Applied Energy, 53, 299-314.

Mandhane, J. M., Gregory, G. A., and Aziz, K. (1974). A flow pattern map for gas-liquid flow in horizontal pipes: predictive models. Int. J. Multiphase Flow, 1, 537-553.

Manfield, P. D. (2000). Experimental, computational and analytical studies of slug flow. PhD thesis, Imperial College of Science, Technology and Medicine, London.

Mao, Z., and Dukler, A. E. (1991). The motion of Taylor bubbles in vertical tubes. II. Experimental data and simulations for laminar and turbulent flow. Chem. Eng. Sci., 46, 2055-2075.

Menter, F. R. (2002). CFD best practice guidelines for CFD code validation for reactor safety applications. EC project ECORA, report EVOL-ECORA-D01.

Menter, F. R. (1993). Zonal two-equation k-ω turbulence models for aerodynamic flows. AIAA, 93-2906.

Moe, R. (1992). Transient simulation of 2-3D stratified and intermittent two-phase flows. PhD thesis, University of Oslo.

Odozi, U. A. (2000). Three-phase gas/liquid/liquid/ slug flow. PhD thesis, Imperial College of Science, Technology and Medicine, London.

Pan, L. (1996). High pressure three phase (gas/liquid/liquid) flow. PhD thesis, Imperial College of Science, Technology and Medicine, London.

Soleimani, A., and Hanratty, T. J. (2003). Critical liquid flows for the transition from the pseudo-slug and stratified patterns to slug flow. Int. J. of Multiphase Flow, 29, 51-67.

Sonnenburg, H. G., Palazov, V., and Dräger, P. (1993)., UPTF-TRAM Versuchsgruppe A, Analyse ausgewählter Versuche. UPTF Fachtagung IV, 25/03/1993, GRS, Mannheim.

Sühnel, T. (2003). Aufbau und Inbetriebnahme eines horizontalen Luft-Wasser-Strömungskanals. Diplomarbeit, Institut für Sicherheitsforschung, FZ Rossendorf, Dresden.

Ubbink, O. (1997). Numerical prediction of two fluid systems with sharp interfaces. PhD thesis, Imperial College of Science, Technology and Medicine, London.

Ujang, P. M. (2003). A three-dimensional study of Taylor bubble turning in two-phase down flow. Second MIT conference on computational fluid and solids mechanics, Elsevier Science Ltd., Ed.: K.J. Bathe, 1176-1180.

Wilcox, D. C. (1994). Turbulence modelling for CFD. La Cañada, California: DCW Industries Inc.

Woods, B. D., and Hanratty, T. J. (1999). Influence of Froude number on physical processes determining frequency of slugging in horizontal gas-liquid flows. Int. J. of Multiphase Flow, 25, 1195-1223.

8. Indexes

8.1 Nomenclature and abbreviations

Notations

Notation	Unit	Denomination
A	m^2	projected area of the body in the direction of flow
A	m^{-1}	interfacial area density
B	-	model parameter (damping of turbulent diffusion)
C_D	-	dimensionless drag coefficient
d	m	interfacial length scale
D_h	m	hydraulic diameter
F_d	N	drag force
g	m/s²	gravity vector
h	m	water level
H	m	channel height
J	m/s	superficial velocity
L	m	channel length
P_{kb}	kg/s²	buoyancy production term (full buoyancy model)
Pr	-	Prandtl-number
t	s	time
U	m/s	velocity
x	m	x coordinate (channel width)
y	m	y coordinate (channel height)
z	m	z coordinate (channel length)

Greek notations

Notation	Unit	Denomination
Δn	-	typical grid cell size across the interface
ρ	kg/m³	fluid density
μ	$kg.m^{-1}.s^{-1}$	viscosity

Indexes

Notation	Denomination
f	index for test facility
G	index for gaseous phase
L	index for liquid phase
m	index for CFD-model
t	index for turbulent

Abbreviations

Notation	Denomination
CCFL	Counter-Current Flow Limitation
CFD	Computational Fluid Dynamics
ECC	Emergency Core Cooling
FZD	Forschungszentrum Dresden-Rossendorf
HAWAC	Horizontal Air/Water Channel
LES	Large Eddy Simulation
LOCA	Loss Of Coolant Accident
PIV	Particle Image Velocimetry
PWR	Pressurised Water Reactor
RPV	Reactor Pressure Vessel
SST	Shear Stress Transport
TOPFLOW	Transient Two Phase Flow Test Facility
VOF	Volume Of Fluid

8.2 Figures

8.3 Tables